DLR-IB-FT-BS-2021-254

Analysis and comparison of the performance of satellite navigation procedures from flight test data at Zurich Airport

Interner Bericht
Hochschulschrift

Autor: Cesario Bergamin
Zeshan Khan

Deutsches Zentrum
für Luft- und Raumfahrt

Institutsbericht
IB 111-2021/254

Analysis and comparison of the performance of satellite navigation procedures from flight test data at Zurich Airport

Cesario Bergamin
Zeshan Khan

Institut für Flugsystemtechnik
Braunschweig

065	Seiten
025	Abbildungen
006	Tabellen
048	Referenzen

Deutsches Zentrum für Luft- und Raumfahrt e.V.
Institut für Flugsystemtechnik
Abteilung Flugdynamik und Simulation

Stufe der Zugänglichkeit: I, Allgemein zugänglich: Der Interne Bericht wird elektronisch ohne Einschränkungen in ELIB abgelegt. Falls vorhanden, ist je ein gedrucktes Exemplar an die zuständige Standortbibliothek und an das zentrale Archiv abzugeben.

Braunschweig, den 11.06.2021

[redacted]

Institutsdirektor:	Prof. Dr.-Ing. S. Levedag
Abteilungsleiter:	Dr.-Ing. H. Duda
Betreuer:	Dr.-Ing. F. Abdelmoula
Verfasser:	Cesario Bergamin Zeshan Khan

Zurich University
of Applied Sciences

School of Engineering

ZAV Centre for Aviation

Deutsches Zentrum
für Luft- und Raumfahrt
German Aerospace Center

Bachelor thesis

(Aviation, Technical Engineering)

Analysis and comparison of the performance of satellite navigation procedures from flight test data at Zurich Airport

Authors	Cesario Bergamin Zeshan Khan
Main supervisor	Dr. Michael Felux
Industrial partner	German Aerospace Center (DLR)
External supervisor	Dr. Fethi Abdelmoula
Date	11.06.2021

DECLARATION OF ORIGINALITY
Bachelor's Thesis at the School of Engineering

By submitting this Bachelor's thesis, the undersigned student confirms that this thesis is his/her own work and was written without the help of a third party. (Group works: the performance of the other group members are not considered as third party).

The student declares that all sources in the text (including Internet pages) and appendices have been correctly disclosed. This means that there has been no plagiarism, i.e. no sections of the Bachelor thesis have been partially or wholly taken from other texts and represented as the student's own work or included without being correctly referenced.

Any misconduct will be dealt with according to paragraphs 39 and 40 of the General Academic Regulations for Bachelor's and Master's Degree courses at the Zurich University of Applied Sciences (Rahmenprüfungsordnung ZHAW (RPO)) and subject to the provisions for disciplinary action stipulated in the University regulations.

City, Date:	**Name Student:**	
11.06.2021, Zurich	Cesario Bergamin	[redacted]
11.06.2021, Zurich	Zeshan Khan	

Acknowledgements

First of all, we would like to thank Dr. Michael Felux for his continuous support in supervising this thesis. It was a pleasure working with him being the supervisor for our project's and bachelor's thesis during the two semesters!

We would also like to thank Dr. Pascal Truffer from Skyguide for his support in providing the GBAS data from the GBAS at Zurich Airport, Dr. Fethi Abdelmoula from the German Aerospace Center (DLR) for the provision of the flight test data and the support with data processing, Mr. Natali Cacciopoli from the Eurocontrol Pegasus team for his support with the Pegasus tool and data processing, Dr. Maurizio Scaramuzza for his relevant inputs in the preparation of this thesis and Gianni Orsatti for the inputs from a pilot's perspective regarding GBAS and SBAS experiences.

Zusammenfassung

Prognosen sagen mittel- und langfristig eine steigende Anzahl von Flugbewegungen voraus, was zu einer Überlastung der bereits stark ausgelasteten Flugsicherungssektoren und Flughäfen in Regionen wie Mitteleuropa führt. Ein Lösungsvorschlag für dieses Problem ist die Einführung von Globalen Navigationssatellitensystemen (GNSS) als primäre Navigationsmittel, die einen flexibleren und effizienteren Betrieb ermöglichen, insbesondere für die Führung von Flugzeugen bei Präzisionsanflügen. Augmentierungssysteme für die Satellitennavigation wie das Ground Based Augmentation System (GBAS) oder das Satellite Based Augmentation System (SBAS) können die Anforderungen an die Navigationsleistung für solch kritische Phasen des Fluges erfüllen, vor allem die Integrität und die Genauigkeit für die sichere Führung des Flugzeugs. Daher konzentrieren sich die Forschungsfragen dieser Arbeit auf die Integritätsleistung in Bezug auf die Protection Levels von GBAS und SBAS und die Genauigkeit der Positionslösung von GBAS, SBAS und Standalone Signalen des Globalen Positionsbestimmungssystem (GPS).

Diese Bachelorarbeit wurde im Rahmen der Erlangung des Bachelorabschlusses im Studiengang Aviatik mit dem Schwerpunkt Technical Engineering verfasst. Die Daten werden vom Deutschen Zentrum für Luft- und Raumfahrt (DLR), Skyguide und dem European Geostationary Navigation Overlay Service Data Access Service (EDAS) zur Verfügung gestellt. Das Ziel dieser Arbeit ist es, aufzuzeigen, wie sich ein operationelles GBAS und SBAS in Bezug auf das Funktionsprinzip, die differentielle Korrekturleistung, die Integritätssicherung und die operationellen Anforderungen unterscheiden.

In einem ersten Schritt wird der für diese Fragestellung notwendige theoretische Hintergrund erarbeitet. Anschliessend werden Testflüge am Flughafen Zürich untersucht und die entsprechenden Daten evaluiert. Die untersuchten Daten liefern die Antworten auf die Forschungsfragen, womit, basierend auf den aktuellen Betriebsleistungen, das Potenzial für zukünftige Anwendungen und Verbesserungen der Systeme bewertet werden kann.

Die Analyse hat gezeigt, dass GBAS im Vergleich zu SBAS eine höhere Leistung in Bezug auf die Genauigkeit der Positionslösung bietet. Beide Systeme können die Genauigkeit von Standalone GPS-Positionslösungen jedoch deutlich verbessern. Bezüglich der Integrität ist die Leistung der Protection Levels von GBAS im Vergleich zu SBAS ebenfalls besser, und die Tatsache, dass die Protection Levels stark von der Satellitengeometrie und der Anzahl der verwendeten Satelliten abhängen, wird in der Analyse gestützt. Die Analyse kommt zu dem Schluss, dass GBAS ideal für die Implementierung auf großen Flughäfen mit mehreren Start- und Landebahnen und Betriebskonzepten ist, während die SBAS-Implementierung deutlich kostengünstiger ist, da sie keine Bodeninstallationen erfordert. Daher ist SBAS für kleinere Regionalflughäfen mit wenigen Start- und Landebahnen und wenigen Betriebskonzepten wirtschaftlich attraktiver.

Abstract

Forecasts predict an increased number of air traffic movements in the mid- and long-term, which results in intermediate congestions of already busy air traffic control sectors and airports in regions such as central Europe. A proposed solution to this consequence is the introduction of Global Navigation Satellite Systems (GNSS) as primary means of navigation, allowing more flexible and efficient operations, especially for the guidance of aircraft on precision approaches. Augmentation systems for satellite navigation such as the Ground Based Augmentation System (GBAS) or the Satellite Based Augmentation System (SBAS) can provide the navigation performance requirements for such critical phases of the flight, mainly the integrity and the accuracy for the safe guidance of the aircraft. Therefore, this bachelor's thesis focuses on the integrity performance in terms of protection levels of GBAS and SBAS and the accuracy performance of the position solution of GBAS, SBAS and unaugmented Global Positioning System (GPS) signals.

This thesis is composed in the context of achieving the bachelor's degree in Aviation with a focus on Technical Engineering. The data is provided by the German Aerospace Center (DLR), Skyguide and the European Geostationary Navigation Overlay Service Data Access Service (EDAS). The goal of this thesis is to illustrate the difference between operational GBAS and SBAS in terms of operating principle, differential correction performance, integrity assurance and operational requirements.

First, the theoretical background necessary to understand the context of the research questions has been assessed. Furthermore, test flights at Zurich Airport were investigated and the data evaluated. The gathered data provides answers to the research questions and implies the potential for future applications and improvements of the systems, based on the current operational performances.

The analysis shows that GBAS provides greater performance in terms of accuracy of the position solution compared to SBAS. Both systems significantly improve the accuracy of the unaugmented GPS position solution. In terms of integrity, the protection level performance of GBAS is better compared to SBAS. Also, the analysis supports the fact that the protection levels strongly depend on the satellite geometry and the number of satellites in use. The analysis concludes that GBAS is ideal for implementation at large airports with multiple runways and operating concepts, whereas SBAS implementation is significantly cheaper as it does not require ground installations. Hence, SBAS is economically more attractive for smaller regional airports with few runways and few operating concepts.

Table of Contents

List of Figures

List of Tables

List of Symbols

Symbol	Unit	Description
$1_{(n)}$	m	Estimated line of sight from the position of the user to a satellite as a vector
λ	m	Wavelength of the carrier phase
τ	s	Filter time constant
ρ_k	m	Current raw pseudorange measurement
"^"		This represents the smoothing of pseudorange values
$\hat{\rho}_{air,corr,t}(n)$	m	Corrected smoothed pseudorange at the aircraft receiver
$\hat{\rho}_{air,t}(n)$	m	Measured smoothed pseudorange at an epoch time t
$\hat{\rho}_i(m.n)$	m	Smoothed pseudorange from the receiver m to the satellite n
$\hat{\rho}_k$	m	Current carrier-smoothed pseudorange
$\hat{\rho}$	m	Smoothed pseudorange
$\Delta\rho(n)$	m	Residuals between the measured and the calculated ranges
ε_p		Noise of code measurement
ε_ϕ		Noise of carrier phase measurement
η_p		Time-varying hardware bias (Code measurement)
η_ϕ		Time-varying hardware bias (Carrier phase measurement)
σ		Standard deviation of Gaussian distribution, index determines application
ϕ_k	m	Current carrier phase measurement input
$\lvert B_{k,apr,lat}\rvert$		Projection of the B-values onto the lateral component
$\lvert B_{k,apr,vert}\rvert$		Projection of the B-values onto the vertical component
b_u	s	User clock offset
d_{major}	m	Error uncertainty along the semimajor axis of the error ellipse
e		Ephemeris error
f	Hz	Frequency of the signal
G		Geometry matrix of line-of-sight vectors between user position and satellites and clock offset matrix
H_1		Single fault case in the ground system for protection level
H_{eph}		Ephemeris protection level
H_o	Hz	Fault-free case for protection level

HAL	m	Horizontal Alert Limit
HPL	m	Horizontal Protection Level
I	m	Ionospheric delay
IC		Correction factor for the ionosphere
k_{ffmd}	m	Fault free missed detection multiplier
k_{md}		Missed detection multiplier
LAL	m	Lateral Alert Limit
LPL		Lateral Protection Level
MP_{ρ}		Code multipath
$MP_{\phi,i}$		Phase multipath
$N_i \lambda_i$	m	Integer ambiguity for the incoming carrier wavelength λ on frequency i
PR	s	Satellite clock correction
PRC		Pseudorange correction
RRC	m	Range rate correction
r	m	Geometric range from the user to the satellite
S		Weighted least-squares projection matrix
$s_{vert,n}$		Scalar parameter describing the weight which is given to the measurement of satellite n (vertical)
$s_{lat,n}$		Scalar parameter describing the weight which is given to the measurement of satellite n (lateral)
t_{zcount}	s	Time at which the correction was calculated
t_{rec}	s	Time of the observable
Δt_{SV}	s	Satellite clock offset
T		Tropospheric delay
TC		Correction factor for the troposphere
TEC	10^{16}el/m^2	Electron density along the signal path
TTA		Time to Alert
VAL	m	Vertical Alert Limit
VPL	m	Vertical Protection Level
w_n		Weighting of the respective satellite n
W		Weighting Matrix

List of Acronyms

AL	Alert Limit
APV	Approach Operation with vertical guidance
ATM	Air Traffic Management
Category-I/II/III PA	CAT-I/II/III Precision Approach
DH	Decision Height
DLR	German Aerospace Center
DOP	Dilution of Precision
EDAS	Geostationary Navigation Overlay Service Data Access Service
EGNOS	European Geostationary Navigation Overlay Service
ENU	East, North, Up Frame
FMS	Flight Management System
GAGAN	GPS Aided GEO Augmentation System
GBAS	Ground Based Augmentation System
GEO	Geostationary Satellite
GIVE	Grid Ionospheric Vertical Error
GLONASS	Globalnaja nawigazionnaja sputnikowaja Sistema
GNSS	Global Navigation Satellite Systems
GPA	Glide Path Angle
GPS	Global Positioning System
GS	Glideslope
GUS	Ground Uplink Station
HAL	Horizontal Alert Limit
HDOP	Horizontal Dilution of Precision
HMI	Hazardously Misleading Information
HPL	Horizonal Protection Level
IFR	Instrument Flight Rules
IGP	Ionospheric Grid Point
ILS	Instrument Landing System
IPP	Ionospheric Pierce Point
IRNSS	Indian Regional Navigation Satellite System
LAL	Lateral Alert Limit
LOC	Localizer
LPL	Lateral Protection Level

LPV	Localizer Performance with Vertical Guidance
LSMD	Dübendorf Air Base
LSZH	Zurich Airport
MCC	Mission Control Center
MEO	Medium Earth Orbit
MI	Misleading Information
MSAS	MTSAT Satellite Based Augmentation System
NLES	Navigation Land Earth Station
NPA	Non-Precision Approach
NSE	Navigation System Error
NSV	Number of Satellites Used
PA	Precision Approach
PL	Protection Level
PRC	Pseudorange Correction
PRN	Pseudo-Random-Noise
RIMS	Ranging Integrity Monitoring Station
RNP	Required Navigation Performance
RQ	Research Question
RSMU #1	Remote Satellite Measurement Unit #1
SBAS	Satellite Based Augmentation System
SCA	Smooth Clock Adjust
SESAR	Single European Sky Air Traffic Management Research
SIS	Signal in Space
TDOP	Total Dilution of Precision
TEC	Total Electron Content
TTA	Time to Alert
UDRE	User Differential Range Error
UHF	Ultra High Frequency
VAL	Vertical Alert Limit
VDB	VHF Data Broadcast
VDOP	Vertical Dilution of Precision
VHF	Very High Frequency
VPE	Vertical Position Error
VPL	Vertical Protection Level
WAAS	Wide Area Augmentation System

1 Introduction

Air transport activity of passengers and cargo increased over the last century and forecasts expect an average growth of 4.3 % per annum over the next 20 years [1]. Despite the current impact of the global pandemic due to COVID-19, air transport movements are still expected to increase in the mid- and long-term. The growing air traffic movements result in intermediate congestions of already busy air traffic control sectors over regions such as central Europe. This development leads to a challenging environment in terms of airspace and airport capacity. Furthermore, during low visibility operations, spacing between arriving aircraft and aircraft operating on ground must be increased, leading to an additional restriction of capacity around airports. Development programs such as Europe's Single European Sky Air Traffic Management Research (SESAR) or the United States' NextGen design Air Traffic Management (ATM) solutions aim to ensure improved operations in such conditions, as the current bottlenecks may lead to significant delays at certain airports that usually then propagate through the network. [2]. One proposal is the increasing use of Global Navigation Satellite Systems (GNSS), such as the United States' Global Positioning System (GPS) constellation, as primary means of navigation. With the use of GNSS as means of navigation, performance in terms of accuracy and integrity can be improved significantly compared to conventional navigation aids mostly used today. The navigation performance requirements differ depending on the phase of the flight, with the strictest ones applying to the guidance of aircraft on precision approaches and during automatic landings. Currently, for these phases of flight, aircrafts are mostly guided by the Instrument Landing System (ILS). However, the ILS can only provide straight-in guidance and requires operational mitigation of signal distortions by significant spacing of the aircraft aligned on the approach. Furthermore, it can only provide approaches at one predefined glide slope angle to one fixed aiming point of the runway. Alternatives to the ILS are GNSS dependent systems such as the Satellite Based Augmentation System (SBAS) or the Ground Based Augmentation System (GBAS), which meet the required performance by providing differential correction for the GNSS signals to improve accuracy, and to provide integrity and continuity for the precision approach service. SBAS allows approaches down to a Decision Height (DH) of 200 ft (Localizer Performance with Vertical Guidance (LPV-200) in SBAS terminology), while GBAS is currently certified for Category I (CAT-I) precision approaches with a DH of 200 ft [3]. GBAS is developed and standardized to also support commercial CAT-II and CAT-III operations in the near future. Both, GBAS and SBAS are GNSS safety critical systems for civil aviation that share similar principles, such as the mentioned differential correction, integrity monitoring and precision approach guidance provided by GNSS. The main difference is that GBAS provides local corrections to the GNSS signals using just ground infrastructure on the airport to which approach service is provided, whereas SBAS broadcasts corrections to the different components of the pseudorange error valid for an area as big as a continent. However, covering such a large area means that the SBAS infrastructure needs tens of sensors distributed in the service area and two or more geostationary satellites (GEOs) to broadcast the information [4]. Examples for SBAS are the Wide Area Augmentation System (WAAS), which covers the contiguous United States, Mexico and Canada or the European Geostationary Navigation Overlay Service (EGNOS), which covers Europe and Northern Africa [5]. The expected benefits from GBAS and SBAS implementation over the ILS involve the improvement of safety through the geometric vertical guidance for final approach, increase of airspace capacity through flexibility, reduction of noise through different glide path angles, reduction of CO_2 emissions through continuous descent approaches and improvement of operational efficiency through shorter flight paths and multiple runway aiming points potentially reducing taxi times [6]. Also, the operational cost can be reduced since GBAS requires only one ground station per airport for operations at every runway from both directions (and technically also other airports in a radius of 42 km around the ground station [7]), whereas the ILS requires one Localizer (LOC) and one Glideslope (GS) per runway end to which approach service is provided. SBAS on the other hand is free from direct user charges worldwide and has the potential to reduce operational costs through the increased options for alternate runways, lower fuel load requirements and increased dispatch reliability [2].

1.1 Situation at Zurich Airport

Currently, Zurich Airport (LSZH) supports Instrument Flight Rules (IFR) approaches with ILS, VOR/DME, GBAS and SBAS [8].

The GBAS station was implemented on the 10th of March, 2011 [9], although only around 3 approaches per day are performed using GBAS [10]. This low number mainly results from the low equipage rate with GBAS avionics of the fleet operating into and from LSZH. Also, currently GBAS only supports ILS-lookalike CAT-I operations on runway 14, whereas the ILS supports operations up to CAT-III on runway 14 and 16. Thus, with the further development of GBAS, it is anticipated to someday replace the ILS as a primary approach guidance system at LSZH, providing more flexible operations, reducing congestion-related delays and ultimately increase the airports capacity.

SBAS approaches with EGNOS are operational at LSZH since 2017, where an LPV-200 procedure was implemented for approaches to runway 14 in 2017 and an LPV procedure with a DH of 670 ft (due to terrain) was implemented for approaches to runway 28 in 2018 [11]. By 2023, SBAS LPV-200 procedures are planned to be implemented for approaches on runways 16 and 34. Currently, SBAS approaches in Zurich are mostly used by corporate aviation, since these aircraft are generally LPV-200 approved, compared to the airliners, where LPV capability is mostly optional [2]. Switzerland's home carrier SWISS currently operates 30 Airbus A220, which are the only SBAS-capable aircraft in their fleet [11] [12].

1.2 Objectives of this Work

The general objective of this work is to analyse and compare the accuracy and integrity performance of commercially operational GBAS and SBAS procedures at LSZH. This can be seen in the context of evaluating the future potential of GBAS and SBAS based on the current performance of both augmentation systems. This is achieved by investigating flight test data of real-world operations with the use of the PEGASUS tool by EUROCONTROL. The general objective of this thesis is split in to two Research Questions (RQ), which shall be answered in the discussion:

RQ1	How does the integrity performance in terms of protection levels of an operational GBAS and SBAS compare in real world operations during a flight test?
RQ2	How does the performance in terms of position solution accuracy of the GBAS, SBAS and standalone single frequency GPS compare?

Table 1, Research questions.

RQ1 focuses on the integrity of GBAS and SBAS, where the protection levels of both systems are compared with the respective alert limits and flight path during the test period. Also, correlations between number of satellites used, satellite geometry and the protection levels are investigated. For SBAS, an integrity diagram is composed to visualize the performance.

RQ2 focuses on the accuracy of the position solutions of GBAS and SBAS, respectively. Through the comparison of the GBAS and SBAS position solution with the standalone GPS position solution, the performance of the differentially corrected GBAS and SBAS positions can be analysed. Additionally, a static antenna in a known location (Remote Satellite Measurement Unit 1 (RSMU #1) at LSZH) is used as a reference location to compare the actual static position with the calculated position solution of the three systems. This is done considering the horizontal and the vertical plane and evaluating a 24 h period to prevent any biased results due to daily dependencies. Additionally, the trajectory of the aircraft calculated by the SBAS is compared with the carrier phase trajectory to assess the positional error calculated by the SBAS in reference to the true position of the aircraft.

This thesis aims to illustrate how the operational GBAS and SBAS differ in terms of operating principle, differential correction performance, integrity assurance and operational requirements. Besides the understanding of relevant theoretical principles, data from real-world flight tests is evaluated. Therefore, the potential for future applications and improvements in the systems will be assessed based on the current operational performances.

1.3 Thesis Outline

After the introduction, the thesis is organized into four main chapters, namely theoretical background, methodology, data evaluation and discussion.

The first chapter provides the theoretical background for the data evaluation by initially giving a brief introduction in the relevant satellite constellation and augmentation system used in this thesis, namely the GPS and EGNOS. The GNSS signals are discussed, elucidating on the signal's components in terms of carrier, the ranging code and the navigation data, as well as the different frequency bands used for the named satellite constellations. In the next subchapter, the operating principle of standalone GNSS signals is explained by discussing the code and carrier phase measurements and the smoothed pseudorange. This section provides the base for the functionality of GBAS and SBAS. Furthermore, the main error sources that adversely influence the performance of GNSS signals are explained. These impairments lead to inaccuracy of standalone GNSS signals and thus, requirements for precision approach guidance cannot be complied with. Therefore, differentially corrected augmentation systems are implemented to reach a performance sufficient for precision approaches. The aviation performance characteristics are stated, focusing on the Signal in Space (SIS) performance requirements, as well as the Required Navigation Performance (RNP) parameters accuracy, integrity, continuity, and availability that distinguish the performance of GNSS augmentation systems from the performance of standalone GNSS signals.

Eventually, the next chapter focuses on the GBAS, discussing the GBAS architecture that consists of the ground subsystem and aircraft subsystem, including the correction generation done at both subsystems, as well as the theory behind the GBAS protection level computation. This is followed by a chapter that focuses on the other augmentation system covered in this thesis, the SBAS. This chapter is structured similar to the previous, discussing the general operating principle, followed by explanations on the SBAS architecture that consists of the reference stations, master stations, ground uplink stations and operational control centres. Also, the theory behind the SBAS protection level computation is briefly discussed.

The last chapter before the data evaluation comprises of the methodology, which covers the methodological approach, methods of data collection, methods of analysis and a justification of the methodological choices for this work.

Furthermore, the data evaluation applies the theory by evaluating flight test data gathered at Zurich Airport. The test flight path and the mission profile are covered, followed by a comparison of the GBAS, SBAS and standalone GPS position solutions. Here, the accuracy is investigated by considering the position solution accuracies and the standard deviations in the vertical and in the horizontal plane. This section covers the second research question that focuses on the accuracy of the systems. Furthermore, the protection levels of GBAS and SBAS over the test period are analysed and compared with the alert limits, and correlations between the number of satellites used, the satellite geometry and the protection levels are discussed. These two sections cover the first research question that focuses on the integrity of the systems. Ultimately, the pseudorange corrections of GBAS and SBAS over a three-hour-period are investigated. This provides a brief overview of the similarities and dissimilarities in the correction generation of both systems.

Finally, the results of the data evaluation are analysed in the discussion, and the findings are summed up in the conclusion. The last part of the thesis is the outlook, where proposals for the further investigation of the topic are given.

2 Background

In this chapter, the theoretical background necessary to understand the context of the research questions is covered. It is divided into the following subchapters: Global Navigation Satellite Systems, Aviation Performance Characteristics, Ground Based Augmentation System and Satellite Based Augmentation System.

2.1 Global Navigation Satellite Systems (GNSS)

Originally designed for warship navigation by the US and USSR military, GNSS are nowadays widely used in the civilian area. Consisting of different satellite constellations, GNSS provide precise navigation based on the principle of multilateration.

2.1.1 Important Satellite Constellations

This chapter is according to [13] and elucidates the satellite constellation and augmentation system used for this thesis.

2.1.1.1 Global Positioning Service (GPS)

The oldest system providing GNSS service is the US GPS that began operations in 1978, currently operating 32 satellites in Medium Earth Orbit (MEO). Its orbits are designed to make at least six satellites visible at any time at all locations on earth, to ensure a continuous, reliable service, providing accuracy of 10 m for the public and 5 m for the military use [13]. Similar systems as GPS are also operated by Russia (Globalnaja nawigazionnaja sputnikowaja Sistema – GLONASS), China (Beidou), India (Indian Regional Navigation Satellite System – IRNSS) and the European Union (Galileo).

2.1.1.2 European Geostationary Navigation Overlay Service (EGNOS)

The EGNOS is a regional European Satellite Based Augmentation System (SBAS) used to improve the performance of GNSS, such as GPS and GALILEO. Its satellite constellation consists of three geostationary satellites, PRN 123, PRN 126 and PRN 136, where PRN 123 and PRN 136 are active, and PRN 126 is currently in testing. It provides safety of life navigation services to aviation, maritime and land-based users. EGNOS uses GNSS measurements taken by reference stations in an accurately known location deployed across Europe and North Africa. These measurements are then taken to a central computing centre where differential corrections and integrity messages are calculated. These calculations are then broadcast using geostationary satellites that serve as an augmentation or overlay to the original GNSS message. Similar SBAS systems commissioned with the same standard as EGNOS also exist in the US (Wide Area Augmentation System – WAAS), Japan (MTSAT Satellite Based Augmentation System – MSAS) and India (GPS Aided GEO Augmentation System – GAGAN) [14]. Currently, 708 EGNOS based procedures at 367 helipads and airports are in use [15].

2.1.2 GNSS Signals

GNSS uses the L-Band which is in the Ultra High Frequency (UHF) part of the frequency spectrum. Satellites continuously transmit navigation signals in two or more frequencies in the L-Band, which ranges from 1 GHz to 2 GHz [16]. These navigation signals contain ranging codes and navigation data that allow users to compute the coordinates of the satellite at any epoch, as well as determine the travel time of the signal from the satellite to the receiver. The main signal components are characterised as follows [17];

The Carrier: Radio frequency sinusoidal signal at a given frequency, onto which the navigation code is modulated with the use of phase modulation.

The Ranging Code: Sequences of 0s and 1s (zeroes and ones), which allow the receiver to determine the travel time of radio signal from satellite to receiver. They are called Pseudo-Random Noise (PRN) sequences or PRN codes.

The Navigation Data: A binary-coded message providing information on the satellite ephemeris (Keplerian elements or satellite position and velocity), clock bias parameters, almanac (with a reduced accuracy ephemeris data set), satellite health status, and other complementary information.

GPS uses the L1, L2 and L5 bands with frequencies of 1575.42 MHz, 1227.6 MHz and 1176.45 MHz, respectively [18], whereas EGNOS uses the L1 Band with a frequency of 1575.42 MHz [14].

2.1.3 Operating Principle

This chapter is according to [19]. The GNSS measurements are based on the propagation time of a signal from a satellite to the receiver to be positioned. In the receiver, the difference between the reception time and the time of transmission is measured. The time of reception is determined by the receiver itself, while the time of transmission is contained in the navigation signals. Multiplying this transmission time by the speed of light, the receiver calculates the so-called pseudorange distance. The pseudoranges are defined as the sum of the true distance between the satellites, the offset of the user clock since the user receiver is not synchronized with the satellite clocks, and the various sources of error. These errors include satellite clock biases, errors introduced by the propagation medium or errors on the receiver side such as multipath and will be explained in Chapter 2.1.4, GNSS Error Sources.

In addition to the navigation code-based pseudorange measurements, the carrier phase of the signals is measured and available as observables at the output of the receiver. Although these measurements are very precise, the number of cycles between the satellite and the receiver is not known and therefore making them equivocal. The code (ρ_i) and carrier phase (ϕ_i) measurement by the true range and including the associated errors for a frequency i are described as

$$\rho_i = r + b_u + T + I_i + e + MP_{\rho,i} + \varepsilon_{p,i} + \eta_{p,i} \tag{1}$$

$$\phi_i = r + b_u + T - I_i + e + N_i\lambda_i + MP_{\phi,i} + \varepsilon_{\phi,i} + \eta_{\phi,i} \tag{1.1}$$

Where r is the geometric range from the user to the satellite, b_u is the user clock offset relative to the satellite time, T is the tropospheric delay, I_i is the ionospheric delay for frequency i, e is the ephemeris error, $MP_{\rho,i}$ and $\varepsilon_{p,i}$ are the code multipath and noise on frequency i, $MP_{\phi,i}$ and $\varepsilon_{\phi,i}$ are the phase multipath and noise on frequency i, $N_i\lambda_i$ describes the integer ambiguity for the incoming carrier wavelength λ on frequency i, and $\eta_{p,i}$ and $\eta_{\phi,i}$ represent the time-varying hardware bias introduced on the code, which can be for example due to the antenna or receiver.

The rate of change of the carrier phase measurements can be used to perform a carrier-smoothing, where the high-frequency noise and multipath from the code measurements can be reduced [20]. The noisy, but unambiguous code pseudorange measurement can be smoothed with the precise, but ambiguous carrier-phase measurements. This carrier-smoothed code measurement is achieved by adding the measurement between two epochs to the previous smoothed pseudorange measurement. These changes in phase measurement can provide an estimate of the change in receiver position over time and in the direction of the satellite generating the phase [21].

The equation for the smoothed pseudorange is described as

$$\hat{\rho}_k = \frac{\Delta t}{\tau}\,\rho_k + (1 - \frac{\Delta t}{\tau})(\hat{\rho}_{k-1} + \lambda(\phi_k - \phi_{k-1})) \tag{2}$$

Where $\hat{\rho}_k$ is the current carrier-smoothed pseudorange, $\hat{\rho}_{k-1}$ is the previous carrier-smoothed pseudorange, ρ_k is the current raw pseudorange measurement, ϕ_k is the current carrier phase measurement input, ϕ_{k-1} is the previous carrier-phase measurement, λ is the wavelength of the carrier phase, Δt is the sample interval and τ is the filter time constant. This Equation (2) is then implemented into the raw pseudorange Equation (1), generating a final equation of the smoothed pseudorange that is formulated as

$$\hat{\rho}_i = r + b_u + \hat{T} + \hat{I}_i + \hat{e} + \widehat{MP}_{\rho,i} + \hat{\varepsilon}_{p,i} + \hat{\eta}_{p,i} \tag{3}$$

where the operator hat "ˆ" represents the corresponding symbols after smoothing. This final smoothed pseudorange $\hat{\rho}$ is an accurate enough measurement to determine the range between the satellite and the receiver. Although multipath and noise error can be minimized, smoothing introduces additional delay through time-variant error sources such as the ionosphere or code hardware biases. Due to the fact that there ultimately are four pseudorange equations (one per satellite), and a minimum of four unknowns, the satellite navigation is a 4-dimensional system with time as the fourth dimension.

2.1.4 GNSS Error Sources

In satellite navigation, there are many different error sources, that strongly differ in their impact on satellite navigation precision and are caused by different sources. These errors can be divided into those originating at the satellite, those originating at the receiver and those that are due to signal propagation by atmospheric refraction. In this Chapter, only the main error sources that have the biggest influence for aviation users are considered.

2.1.4.1 Ionospheric Delay

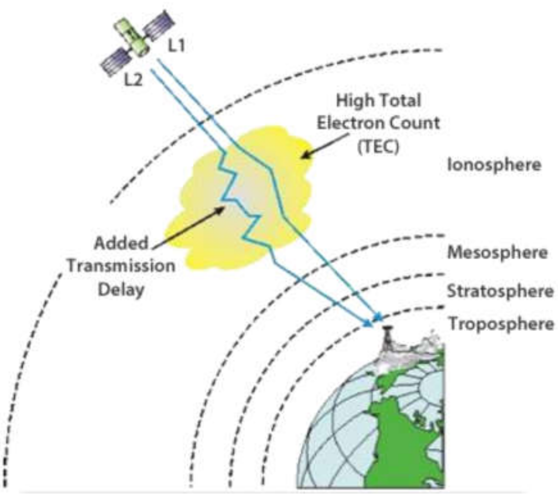

Figure 1, Effects of the Ionosphere on the satellite signal [23].

The ionosphere is an atmospheric layer between around 60 km and 2000 km, containing a large number of ionized particles. It spreads from the mesosphere over the thermosphere to the exosphere. The ultraviolet and x-ray radiation from the sun interacts with the gas molecules and atoms, which leads to gas ionization. This plasma bends ranging signal by refraction and changes their propagation speed as illustrated in Figure 1. The range error d (in meters) introduced by the ionosphere is given in Equation (4), where TEC represents the integrated electron density along the signal path (Total Electron Content) and f is the frequency of a signal i [22].

$$d = 40.3 \cdot \frac{TEC}{f_i^2} \tag{4}$$

The ionospheric delay is inversely proportional to the square of the frequency of the signal, which means that the higher the frequency of the signal, the lower the ionospheric delay. Additional to the range error, the ionosphere also causes a curvature of the signal. Although the curvature of the signal path causes an extremely small, almost negligible range error, the change in propagation speed can already cause significant range errors [22].

Another important point is that the delay of the ionosphere depends on the position of the satellite as seen from the user. If the satellite observed by the user is at the zenith, the signal's path through the ionosphere is shorter than if the satellite is seen at a small elevation angle close to the horizon. This means that the error introduced by the ionosphere for a certain satellite is at its highest when the satellite rises or sets at the horizon as seen from the user and is at its lowest if the satellite is at its zenith relative to the user.

2.1.4.2 Tropospheric Delay

Another atmospheric perturbation is the delay introduced by the troposphere. Although, the variability of the tropospheric impact is much smaller compared to that of the ionosphere. The troposphere is the lowest layer of the atmosphere and goes up from the earth's surface to about 50 km. It consists of dry gas and water vapour and is an electrically neutral layer of the earth's atmosphere, which means it is not ionized. Similar to the ionosphere, the troposphere also extends the time of the signal by refraction and its impact on the satellite signal error depends on the elevation angle of the satellite relative to the user. The total delay can be divided into the wet and the dry component. The dry component, which makes about 90 % of the total error, is a function of pressure and temperature, whereas the wet component is a function of humidity. The dry component is easier to determine than the wet component, which is due to the difficulties in predicting water vapour distribution from surface measurements.

The effect on the satellite signal through the troposphere is different compared to the ionosphere. The troposphere is refracting, where the refraction of the signal is not dependent on the frequency if it is below 30 GHz [24]. Therefore, the known frequency bands of GNSS L1, L2 and L5, are refracted equally. The refraction is equivalent to a delay in the arrival of the signal from a GNSSS satellite. This means that the range between receiver and satellites appears to be greater than it is due to the signal being delayed and taking more time to reach the receiver. The tropospheric delay experienced by a user depends on whether a satellite is at the zenith or at the horizon as seen from the user because the path of the signal through the troposphere is longer when the satellite is at the horizon than when it is at the zenith. Thus, similar to the error introduced by the ionosphere, the quality of positioning with a satellite appearing on the horizon increases until the satellite is at the zenith as seen from the user, and then the accuracy gradually decreases until the satellite disappears behind the horizon.

2.1.4.3 Multipath

Multipath, together with the ionospheric error, is one of the main sources of error in GNSS. Multipath occurs when the antenna receives a signal via multiple paths (a mixture of refracted and direct paths) rather than from a sole direct line of sight, as seen in Figure 2. Refraction usually occurs if a signal is deflected by surfaces such as buildings or other aircraft, or really any reflective surface. These do not necessarily have to be large to cause multipath errors. This combination of multiple paths increases the measurement of the propagation time and thus increases the pseudorange measurement, making the range between the satellite and the receiver seem longer than it actually is [25].

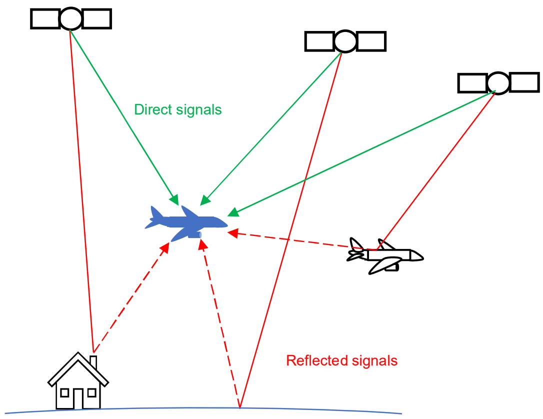

Figure 2, Multipath Effects on the satellite signals (simplified version with ranges not to scale).

2.1.4.4 Satellite Geometry

The satellite geometry is not an actual error source, although it has a direct impact on the quality of the derived position. The accuracy of the satellite navigation is subject to a geometrically defined measure called Dilution of Precision (DOP). The Total DOP (TDOP) can be divided into the Horizontal DOP (HDOP) and the Vertical DOP (VDOP) and it concerns the geometric strength of the position solution described by the positions of the satellites with respect to one another or to the receivers [26]. The lower the DOP value, the more optimal the satellite configuration and therefore the higher the quality of the position derived from them. Figure 3 shows different examples of satellite geometries with 4 satellites in a tetrahedron volume and their respective influence on HDOP and VDOP [27].

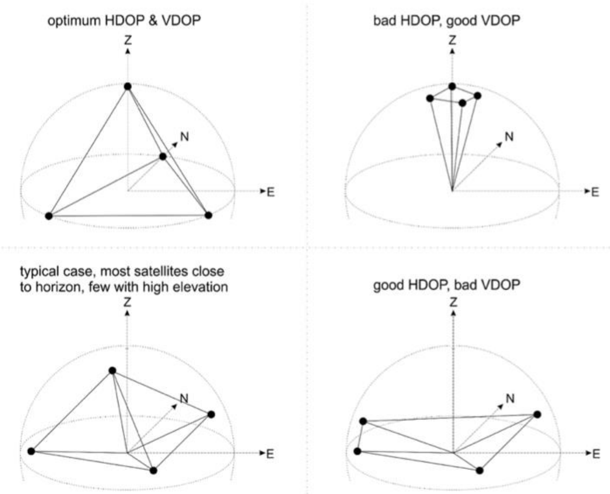

Figure 3, Dilution of precision example: tetrahedron volume with 4 satellites.[27]

Additional to the DOP, the number of satellites available also plays a role in the accuracy of satellite navigation. It can be generally said that the more satellites are visible from the user location, the smaller the contribution of each satellite to the position solution and therefore the smaller the influence of an error generated by a single satellite. The integrity as well as the accuracy can be adversely affected by only using a minimum of four satellites for a position solution, which is why it is optimal to generate a position solution using a larger number of available satellites.

2.2 Aviation Performance Characteristics

In order to provide Signal in Space (SIS) for safe and reliable GNSS operations, four parameters are used: Accuracy, Integrity, Continuity and Availability. Those parameters are defined by ICAO and specify the Required Navigation Performance (RNP) for GNSS operations that have to be met for each phase of the flight. For the GBAS operations, the RNP characterizes both the sole performance of a navigation system and the joint performance of the navigation and flight control systems. Compared to GBAS' and SBAS' four RNP parameters, accuracy is the only of the four parameters that is required to be met for standalone GPS [28]. A complete table of the GNSS SIS requirements is given in Table 2 [29].

<table>
<tr><th>Typical Operations</th><th>Horizontal Accuracy 95 %</th><th>Vertical Accuracy 95 %</th><th>Integrity</th><th>Time to Alert</th><th>Continuity</th><th>Availability</th></tr>
<tr><td>En-route</td><td>3.7 km</td><td>N/A</td><td>$1-10^{-7}$/ h</td><td>5 min</td><td rowspan="3">$1-10^{-4}$ / h to $1-10^{-8}$ / h</td><td rowspan="6">0.99 to 0.99999</td></tr>
<tr><td>En-route, Terminal</td><td>0.74 km</td><td>N/A</td><td>$1-10^{-7}$/ h</td><td>15 s</td></tr>
<tr><td>Initial Approach, Intermediate Approach, Non-Precision Approach and Departure</td><td>220m</td><td>N/A</td><td>$1-10^{-7}$/ h</td><td>10 s</td></tr>
<tr><td>Approach operation with vertical guidance (APV-I)</td><td>16 m</td><td>20 m</td><td>$1-2*10^{-7}$ per approach</td><td>10 s</td><td rowspan="3">$1-8*10^{-6}$ per 15 s</td></tr>
<tr><td>Approach operation with vertical guidance (APV-II)</td><td>16 m</td><td>8 m</td><td>$1-2*10^{-7}$ per approach</td><td>6 s</td></tr>
<tr><td>Category I Precision Approach (CAT-I/LPV-200)</td><td>16 m</td><td>6 to 4 m</td><td>$1-2*10^{-7}$ per approach</td><td>6 s</td></tr>
</table>

Table 2, GNSS SIS performance requirements [29].

2.2.1 Accuracy

Accuracy is measured by the GNSS position error which, according to ICAO, "*is the difference between the estimated position and the actual position. For an estimated position at a specific location, the probability should be at least 95 per cent that the position error is within the accuracy requirement." (ICAO Annex 10)* [29].

The accuracy is subdivided into horizontal and the vertical accuracy and defines the permitted lateral and altitude-dependent deviation for different operations, that have to be met during at least 95 % of the operations. An error in the estimation of an aircraft's position is referred to as Navigation System Error (NSE) and equals the GNSS position error. GPS has the capability to provide accurate position and time information worldwide. The accuracy achieved by this constellation is sufficient to meet aviation requirements for en-route through non-precision approach but not for precision approaches, as seen in see Table 3. This lack of accuracy for precision approaches (especially in the vertical plane) is solved with the use of differential corrections by an augmentation system such as GBAS and SBAS [30].

	GPS global average 95 % of the time	**CAT-I/LPV-200 Precision Approach requirements for 95 % of the time**
Horizontal Position Error	13 m	**16 m**
Vertical Position Error	22 m	**4 to 6 m**

Table 3, GPS Position accuracy and CAT-I/LPV-200 Precision Approach requirements [29].

2.2.2 Integrity

For safety of life applications, such as navigation for automatic landings, not only accuracy is important, but also particularly the integrity.

ICAO defines integrity as "*A measure of the trust that can be placed in the correctness of the information supplied by the total system. Includes the ability of a system to provide timely and valid warnings to the user (alerts)." (ICAO Annex 10)* [29]

For SBAS and GBAS operations, integrity is assured by the introduction of Protection Levels (PL). These PLs are subdivided into the Horizontal/Lateral Protection Level (HPL/LPL) and the Vertical Protection Level (VPL). In the case of GBAS, the PL in the horizontal plane is called Lateral Protection Level (LPL), since it is calculated in flight direction due to the presence of a reference point (GBAS station of the airport) [4]. In the case of SBAS, the PL in the horizontal plane is called Horizontal Protection Level (HPL), since it is calculated in the direction of the large semi-axis due to the absence of a ground station at the airport [22]. These values are conservative bounds of the actual positioning error that can be calculated based on standardized models for different error contributions. Additionally, the integrity of an operation is assured through the Alert Limit (AL). The ALs are the maximum allowable NSE for a certain operation and define what an acceptable position error is. Similar to the HPL/LPL and VPL, the AL is also expressed in a horizontal/lateral and vertical component (HAL/LAL

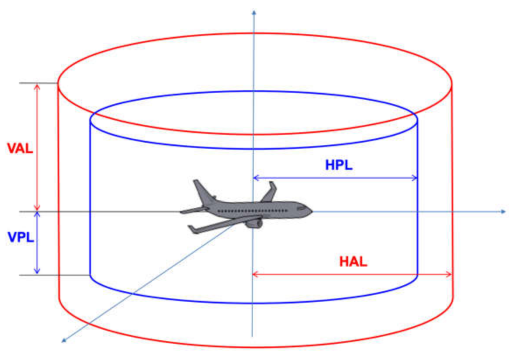

Figure 4, Protection Levels and Alert Limits [31] and VAL respectively) as seen in Figure 4. As long as the values of the PLs, derived from the augmentation signal and satellite pseudorange measurements, remain smaller than those of the ALs, integrity is assured, and a safe operation of the aircraft is guaranteed. The ALs are shown in Table 4.

Typical operation	**Horizontal Alert Limit (HAL)**	**Vertical Alert Limit (VAL)**
En-route (oceanic / continental low density)	7.5 km	N/A
En-route (continental)	3.7 km	N/A
En-route (terminal)	1.85 km	N/A
Non-Precision Approach	556 m	N/A
Approach operation with vertical guidance (APV-I)	40 m	50 m
LPV-200	40 m	35 m
Approach operation with vertical guidance (APV-II)	40 m	20 m
Category I Precision Approach (CAT-I)	40 m	35 to 10 m

Table 4, Horizontal and Vertical Alert Limits for GNSS operations [28].

Additional to the ALs, the integrity of an operation is assured through the introduction of the Time to Alert (TTA), which is the maximum allowable time elapsed from the onset of the navigation system being out of tolerance until the equipment enunciates the alert [31]. The TTA for a certain operation is given in Table 2.

Integrity calculations differ for GBAS and SBAS and are therefore explained in more detail in the respective chapters.

2.2.3 Continuity

According to the ICAO, continuity is defined as *"the capability of the system to perform its function without unscheduled interruptions during the intended operation." (ICAO Annex 10)* [29]

More specifically, the continuity of a system is the probability that the specified system performance will be maintained for the duration of a phase of operation, presuming that the system was available at the beginning of that phase of operation. This parameter is introduced to ensure a continuous quality of service without unscheduled interruptions.

2.2.4 Availability

ICAO defines the availability of GNSS as *"the portion of time the system is to be used for navigation during which reliable navigation information is presented to the crew, autopilot, or other system managing the flight of the aircraft." (ICAO Annex 10)* [29].

Availability describes the probability that the navigation system will be operational during a certain time. A navigation system is considered available for use in a specific flight operation if the PLs it is providing are inferior to the corresponding specified ALs for that same operation (see Figure 5). The red airplane shape represents the actual aircraft position and the distance from this shape to the centre of the circumferences represents the NSE. The availability is measured in the vertical and horizontal plane, and the lower value of both planes represents the total availability of the system. The availability is a function of both the physical characteristics of the environment and the technical capabilities of the transmitter facilities [31].

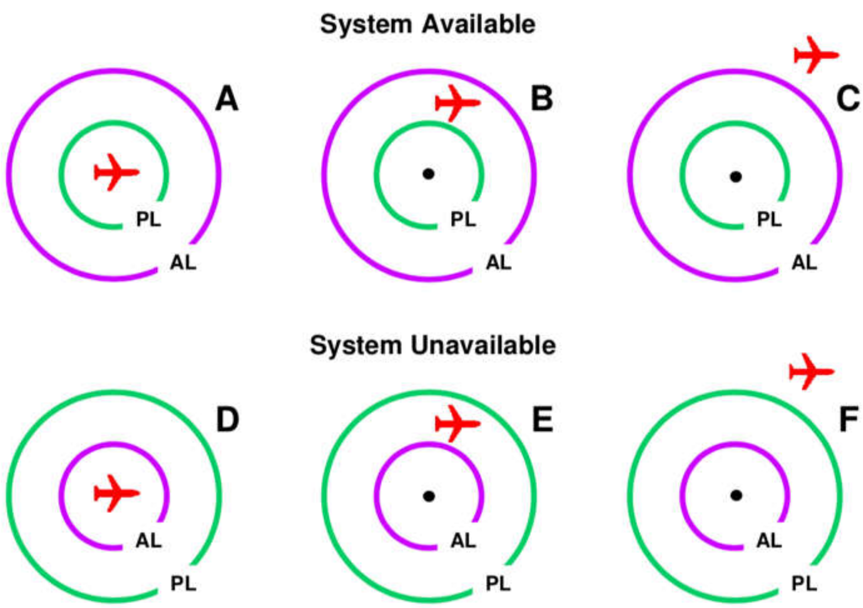

Figure 5, Integrity and Availability Definition [31].

2.3 Ground Based Augmentation System (GBAS)

A Ground Based Augmentation System (GBAS) is a civil-aviation safety-critical system that improves the GNSS navigation system's performances. It supports local augmentation of the primary GNSS constellations by providing approach geometry reference to aircraft, integrity monitoring and generation and transmission of differential corrections of GNSS data with the use of a reference ground station. The goal of a GBAS is to provide signal accuracy, integrity, continuity and availability for aircraft operations [32].

2.3.1 GBAS Architecture

The GBAS infrastructure can be divided into three main components:

- The Satellite Subsystem (GNSS Satellites)
- The Ground Subsystem
- The Aircraft Subsystem

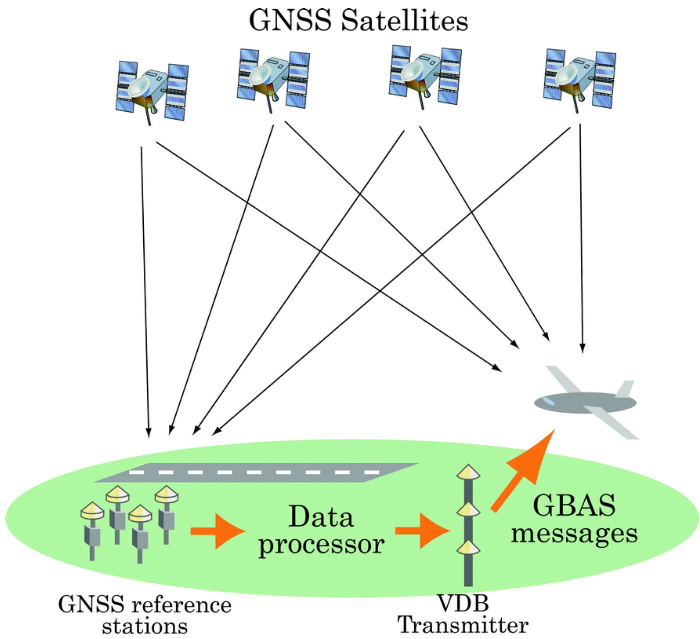

Figure 6, GBAS Architecture consisting of the Satellite Subsystem, Ground Subsystem and Aircraft Subsystem [33].

The satellite subsystem is composed by the GNSS ranging sources and transmits the ranging signals and navigation messages both to the aircraft and to the ground subsystem.

2.3.1.1 Ground Subsystem

A GBAS ground subsystem as seen in Figure 7 normally consists of four GPS antennas, a central processing system (Ground Facility) and a VHF Data Broadcast (VDB) transmitter. These facilities are all located at the airport itself. The ground facility uses a VHF radio link to send data to aircraft that consist of GPS corrections, integrity parameters and approach path information. This radio link operates in the frequency range between 108 MHz and 118 MHz. Each reference receiver measures the propagation errors introduced by atmospheric refraction for its receiver location. The average of these measurements is then applied to the satellite ranges measured by the GBAS avionics which are therefore corrected. The ground facility is also used to monitor general GPS satellite performance such as the satellites health. If a satellite sends incorrect data, the ground facility stops broadcasting from the affected satellite and corrects it with the use of another satellite in order to prevent the transmission of incorrect data to the GBAS avionics on board the aircraft (see Chapter 2.2.2, Integrity). Confidence that the aircraft's calculated and differentially corrected position is accurate is achieved through additional parameters sent by the ground facility. Those parameters are used by the GBAS avionics to determine error bounds on the calculated GPS position. Furthermore, an updated correction message is broadcasted twice a second through the VDB transmitter. These messages contain the corrections and less frequently, integrity parameters, ground facility characteristics and approach path guidance. The VDB broadcasts the signal throughout the GBAS coverage area to the GBAS avionics of the aircraft subsystem. The GBAS provides its service to a local area in which continuous support of the aircraft is provided, from the en-route airspace through the terminal airspace to the precision approach and landing in a radius of about 42 km [7] around the ground station [34].

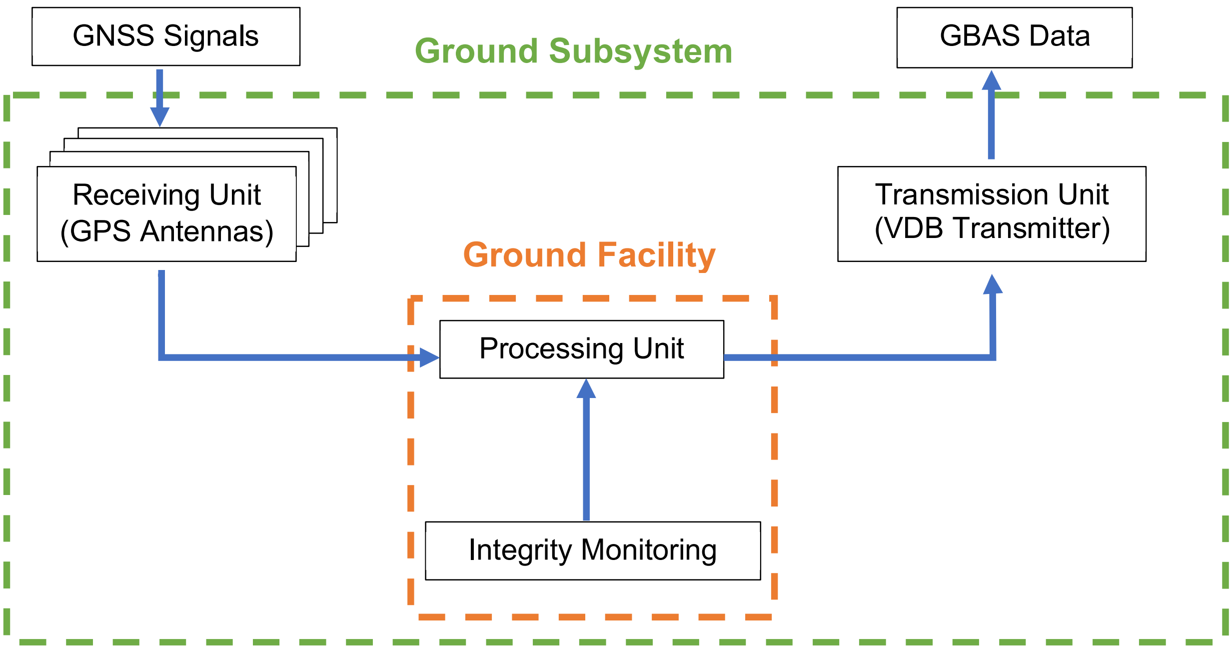

Figure 7, The Ground Subsystem with its Ground Facility, which generates the GBAS corrections.

2.3.1.1.1 Ground Subsystem Correction Generation

The following chapter is according to [19]. With a measurement from a reference receiver, the ground subsystem can calculate a carrier-smoothed pseudorange correction for the satellites in view. The position of the reference antenna is precisely known, which has the advantage that the position of the satellite can be calculated by the use of the navigation message. Therefore, the geometrical range to each satellite in view can be determined.

By subtracting the smoothed pseudorange and the satellite clock bias from the geometric range, a pseudorange correction PRC_{CSC} can be calculated for each candidate:

$$PRC_{CSC}(m,n) = r(m,n) - \hat{\rho}_i(m.n) - c \cdot \Delta t_{SV}(m,n) \tag{5}$$

Where r describes the geometric range from the receiver m to the satellite n, $\hat{\rho}_i(m.n)$ is the smoothed pseudorange, $\Delta t_{SV}(m,n)$ is the clock bias calculated for the satellite n, based on the navigation message received from a user m. The i always describes the frequency in the context.

With the carrier smoothed pseudorange from Equation (3) the PRC_{CSC} can be written as:

$$PRC_{CSC}(m,n) = -c \cdot \Delta t_m - \hat{T} - \hat{I}_i - \widehat{MP}_{\rho,i} - \hat{\varepsilon}_{\rho,i} - \hat{\eta}_{\rho,i} \tag{6}$$

The PRC_{CSC} contains the receiver clock offset, which can be removed by the so-called smooth clock adjust (SCA). The smooth clock adjust removes a weighted average of all pseudorange corrections for a given receiver.

$$PRC_{SCA}(m,n) = PRC_{CSC}(m,n) - \sum_{j=1}^{N} w_j \, PRC_{CSC}(m,j) \tag{7}$$

The formula gives the correction for a receiver m and a satellite n after the smoothed clock adjust, where N is the number of satellites involved and w_j is the weighting of the respective satellite.

With the pseudorange correction, it is possible to calculate a broadcast correction for a satellite n. This broadcast correction is calculated from the average of all pseudorange correction candidates for one satellite over all receivers.

$$PRC_{TX}(n) = \frac{1}{M}\sum_{k=1}^{M} PRC_{SCA}(k,n) \tag{8}$$

To the pseudorange corrections, additional range rate corrections $RRCs$ are broadcasted from the ground. These are calculated as the rate of change of the current and previous transmitted $PRCs$:

$$RRC_{TX,t}(n) = \frac{PRC_{TX,t}(n) - PRC_{TX,t-1}(n)}{\Delta t} \tag{9}$$

2.3.1.2 Aircraft Subsystem

A GBAS aircraft subsystem as seen in Figure 8 normally consists of a GPS antenna, a VHF Data Broadcast (VDB) antenna as well as associated processing equipment. GBAS avionics are standard on all new Boeing aircraft that are delivered these days, and optional on the Airbus A320, A330, A350 and A380. Either the pilot selects a predefined approach from the Flight Management System (FMS), or he enters a five-digit channel number through the pilot's interface in order to access the broadcasted data. The VDB antenna receives the corrections sent by the ground subsystem, namely the VDB transmitter. These corrections are then applied to the pseudorange measurements taken by the GNSS receiver on board the aircraft. Then they are computed through the processing equipment (Processor) in order to gain more accurate GPS position, velocity and time to guide the aircraft safely to the runway. The signal provides guidance, which is similar to the ILS, thus making minimal difference to the aircraft instruments such as the primary flight display or the flight control system [35].

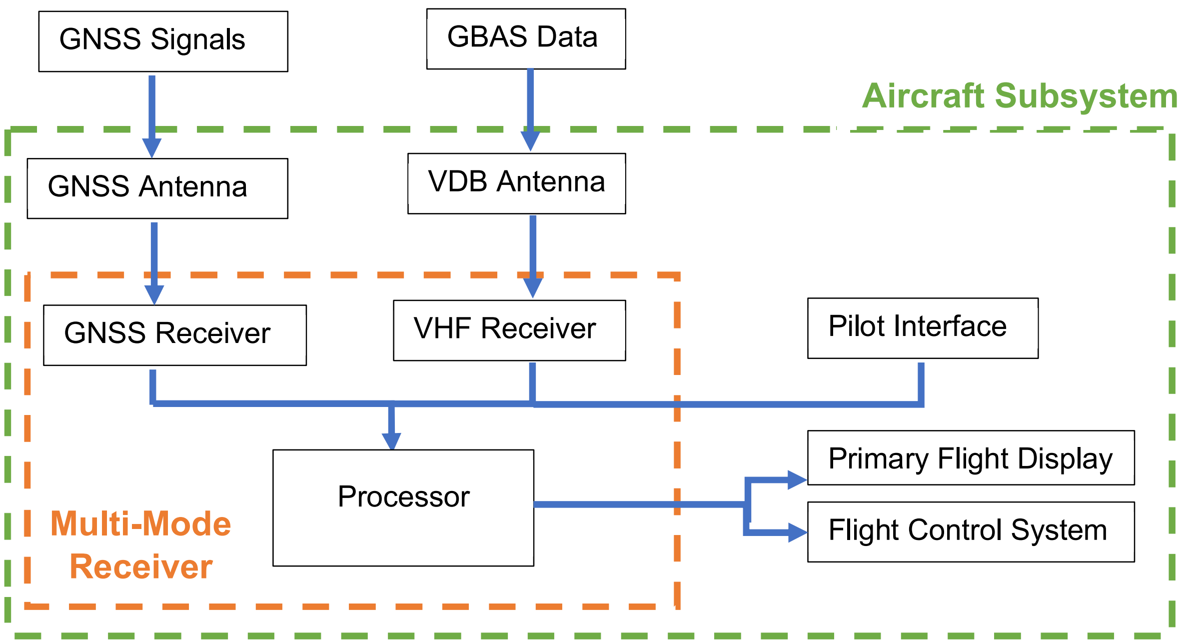

Figure 8, The Aircraft Subsystem with its Multi-Mode Receiver, which applies the GBAS corrections to the GNSS signals.

2.3.1.2.1 Aircraft Subsystems Correction Generation

The following chapter is according to [19]. The aircraft receives the smoothed pseudorange and range rate corrections and uses them to correct its own smoothed pseudorange measurement. The corrected smoothed pseudorange at the aircraft receiver is given as

$$\hat{\rho}_{air,corr,t}(n) = \hat{\rho}_{air,t}(n) + PRC_{TX}(n) + RRC_{TX}(n) \cdot (t - t_{zcount}) + TC + c \cdot \Delta t_{SV} \qquad (10)$$

Where $\hat{\rho}_{air,t}(n)$ is the measured smoothed pseudorange at an epoch time t, $PRC_{TX}(n)$ is the broadcast correction from the ground subsystem, $RRC_{TX}(n)$ is the range rate correction from the related message, TC is the differential tropospheric correction, Δt_{SV} is the satellite clock offset and t_{zcount} describes the time at which the correction was calculated.

By using the pseudorange measurement $\hat{\rho}_{air,t}(n)$ and the corrections broadcast by the ground subsystem it is possible for the user to calculate the position coordinates x(x_u, y_u, z_u) and the clock error $c \cdot \Delta t_u$ by

$$\hat{\rho}_{air,corr,t}(n) = \|x(n) - x\| + c \cdot \Delta t_u + \tilde{\varepsilon}_\rho(n) \qquad (11)$$

A further position x_0 is given by

$$\hat{\rho}_0(n) = \|x(n) - x_0\| + c \cdot \Delta t_u + \tilde{\varepsilon}_\rho(n) \qquad (12)$$

This equation calculates an estimated position, which is made by the last known position.

In a next step the residuals $\Delta\rho(n)$ between the measured and the calculated ranges are calculated by linearization using the Taylor series.

$$\Delta\rho(n) = \hat{\rho}_{air,corr,t}(n) - \hat{\rho}_0(n) = -1_{(n)}\Delta x + \Delta b + \tilde{\varepsilon}_\rho(n) \qquad (13)$$

where $1_{(n)}$ is the estimated line of sight from the position of the user to a satellite as a vector.

If the sight line vector is inserted into the geometry matrix, Equation (13) can be written as:

$$\Delta\rho = G\begin{bmatrix}\Delta x\\ \Delta b\end{bmatrix} + \tilde{\varepsilon}_{\rho} \tag{14}$$

This equation can be solved iteratively. The solution is done by moving the linearization point according to the least-squares solutions for the parameters to be estimated. When measuring the satellite broadcast, different levels of noise can occur. These noise intensities depend on factors such as the elevation angle of the satellite relative to the user. An additional weighting is introduced, which gives more weight to satellites where fewer measurement errors are expected. The parameters to be estimated are then calculated using a least square approach.

$$\begin{bmatrix}\Delta x\\ \Delta b\end{bmatrix} = \left(G^{T}WG\right)^{-1}G^{T}W\Delta\rho = S\Delta\rho \tag{15}$$

$$S = (G^{T}WG)^{-1}G^{T}W \tag{15.1}$$

In Equation (15), S describes the weighted least-squares projection matrix. The projection factors relating the GNSS measurements from satellite n to the position domain in approach coordinates play an important role in the integrity assurance process, and the contribution of a single satellite n to the position estimate vertical to the approach track is given by

$$s_{vert,n} = s_{3,n} + s_{1,n} \cdot \tan{(GPA)} \tag{16}$$
$$s_{lat,n} = s_{2,n}$$

Where $s_{vert,n}$ and $s_{lat,n}$ are vertical and horizontal scalar parameters describing the weight, which is given to the measurement of satellite n, $s_{k,i}$ are the entries of the S-Matrix of row k and column i and GPA is the glide path angle of the approach. As seen in Chapter 2.1.4.4, Satellite Geometry, it can be generally assumed that the more satellites are available for GBAS corrections, the lower the s_{vert} value and therefore the lower the impact of a pseudorange measurement error by a single satellite n on the position solution.

The weighting matrix W is the inverse of the covariance matrix of the measurements and is described as

$$W = \begin{bmatrix}\sigma_1^2 & 0 & 0 & 0\\ 0 & \sigma_2^2 & 0 & 0\\ \dots & \dots & \dots & \dots\\ 0 & 0 & 0 & \sigma_n^2\end{bmatrix} \tag{17}$$

The weighting matrix contains the differences of the variances of the measurement errors from the different satellites and σ^2 is the variance of the differential corrected pseudorange measurements.

2.3.2 GBAS Protection Level Computation

This chapter is according to [19] and only considers the PL computations of GBAS CAT-I precision approaches. Three PLs are calculated: one for the fault-free case (H_o), one for a single fault case in the ground system (H_1) and an ephemeris protection level (H_{eph}), which will not be discussed further in the scope of this work.

The fault-free protection levels H_0 are influenced by the nominal measurement error models and the satellite geometry. They are defined as

$$VPL_{H_0} = k_{ffmd}\sqrt{\sum\nolimits_1^N s_{apr,vert,n}^2 \cdot \sigma_n^2} \tag{18}$$

$$LPL_{H_0} = k_{ffmd}\sqrt{\sum\nolimits_1^N s_{apr,lat,n}^2 \cdot \sigma_n^2} \tag{19}$$

Where k_{ffmd} represents the fault free missed detection multiplier, $s_{apr,lat}$ represents the projection onto the lateral component for the n-th ranging source and $s_{apr,vert}$ the projection of the vertical component and of the along-track component into the vertical for the same n-th ranging source as defined in Equation (16) and σ_n represents the standard deviation of the uncertainty of the residual differential pseudorange error (consisting of the ground multipath and noise σ_{gnd_x} , the airborne multipath and noise σ_{air}, the residual tropospheric error σ_{tropo} and the residual ionospheric error σ_{iono}) for the satellite n, as described in Equation (20). Thus, the uncertainty of the residual differential pseudorange consists of the root-sum-square of uncertainties introduced by these effects.

$$\sigma_n^2 = \sigma_{gnd\_x}^2 + \sigma_{air}^2 + \sigma_{iono}^2 + \sigma_{tropo}^2 \tag{20}$$

The protection levels in the case of a fault in one of the measurements from the ground receiver are defined for each receiver as

$$VPL_{H_1}[k] = \left|B_{k,apr,vert}\right| + k_{md}\sqrt{\sum\nolimits_1^N s_{apr,vert,n}^2 \cdot \sigma_{H_1,n}^2} \tag{21}$$

$$HPL_{H_1}[k] = \left|B_{k,apr,lat}\right| + k_{md}\sqrt{\sum\nolimits_1^N s_{apr,lat,n}^2 \cdot \sigma_{H_1,n}^2} \tag{22}$$

Where k is the index for the ground reference receiver and k_{md} represents the missed detection multiplier, $\left|B_{k,apr,vert}\right|$ and $\left|B_{k,apr,lat}\right|$ are projections of the B-values onto the vertical and lateral component. The B-values are an estimate of the error contribution from each reference receiver to the corrections provided to the aircraft and are broadcast by the ground and derived from 100 seconds smoothed pseudorange corrections. The standard deviation of the residual differential pseudorange for the one fault case is computed as

$$\sigma_{H_{1,i}}^2 = \sqrt{\frac{M(n)}{U(n)}\sigma_{gnd\_x}^2 + \sigma_{air}^2 + \sigma_{iono}^2 + \sigma_{tropo}^2} \tag{23}$$

where *M* represents the total number of receivers and *U* the number of reference receivers used to compute the correction for the satellite *n* excluding the receiver *k*.

The aircraft computes the maximum among the three PLs and verifies if the values are smaller than the ALs (in both lateral and vertical). In case any of the bounds exceeds the limits, the service becomes unavailable.

2.4 Satellite Based Augmentation System (SBAS)

A Satellite Based Augmentation System (SBAS) is designed to enhance the performance of GNSS positioning by differential corrections, integrity monitoring and ranging. Differential corrections increase the accuracy with position errors below 1 meter [36], integrity monitoring improves the safety whereas the ranging function improves availability and continuity [37].The augmentation information provided by the SBAS covers corrections and integrity for satellite position errors, satellites clock/time errors and errors induced by the estimation for the delay of the signal while crossing the ionosphere. Errors induced by the estimation of the delay caused by the troposphere and its integrity are resolved by the application of a tropospheric delay model [36].

2.4.1 SBAS operating principle

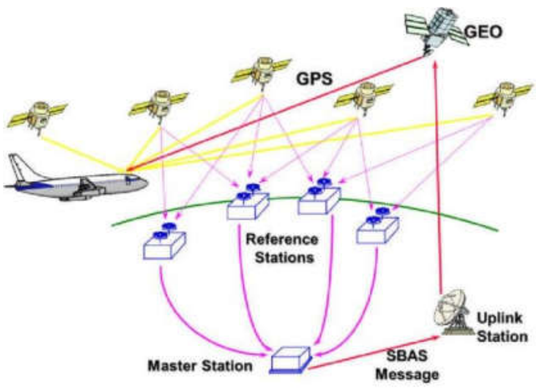

Figure 9, SBAS Architecture consisting of the ground segment and the space segment [38].

This chapter is according to [37]. SBAS utilizes a network of ground monitors to continuously observe the performance of the navigation satellites. Reference stations take measurements by the navigation satellites and send these to the master stations that determine differential corrections and corresponding confidence bounds. This data is then transmitted to the uplink station, which then relays this information to the end user via a GEO, as seen in Figure 9. SBAS consists of several master stations, uplink stations and GEOs to provide redundancy in the case of a failure of any one component.

The augmentation of core constellations is done with three services:

1. Differential Corrections

For each of the navigation satellites tracked by the ground network, differential corrections are broadcasted by the SBAS to the user. Also, over its region of interest, corrections for the ionospheric delay effects are transmitted. These corrections can then be applied to the user's pseudorange measurements and improve the user's position accuracy.

2. Integrity Monitoring

Error bounds for each monitored satellite and each ionospheric correction parameter is broadcasted by the SBAS to the user. These error bounds determine the maximum position error that is acceptable after the differential corrections are applied. The probability that the position error bound fails to overbound the true error must be smaller than 10^{-7} per approach and this information must be updated within 6 seconds of any unsafe condition.

3. Ranging

The SBAS GEO signals are similar to the L1 signals in design. This means that an SBAS-enabled receiver uses the same hardware than a normal GPS receiver. The SBAS signals are synchronized to GPS and therefore they can be used for ranging. With this function the time availability and continuity of the position correction can be improved.

Each master station generates a grid of ionospheric corrections over its coverage region. The grid consists of ionospheric grid points (IGP) and is 5° by 5° in latitude and longitude and less dense over the polar regions, as seen in Figure 10 for the case of EGNOS. It can be seen as a thin shell existing at 350 km above the surface of the earth. The line of sight between the receiver and the navigation satellite penetrates this layer at a point in between four IGPs. This point is labelled as the ionospheric pierce point (IPP). The user applies the four surrounding grid values to interpolate the ionospheric delay specific to each location of their IPPs.

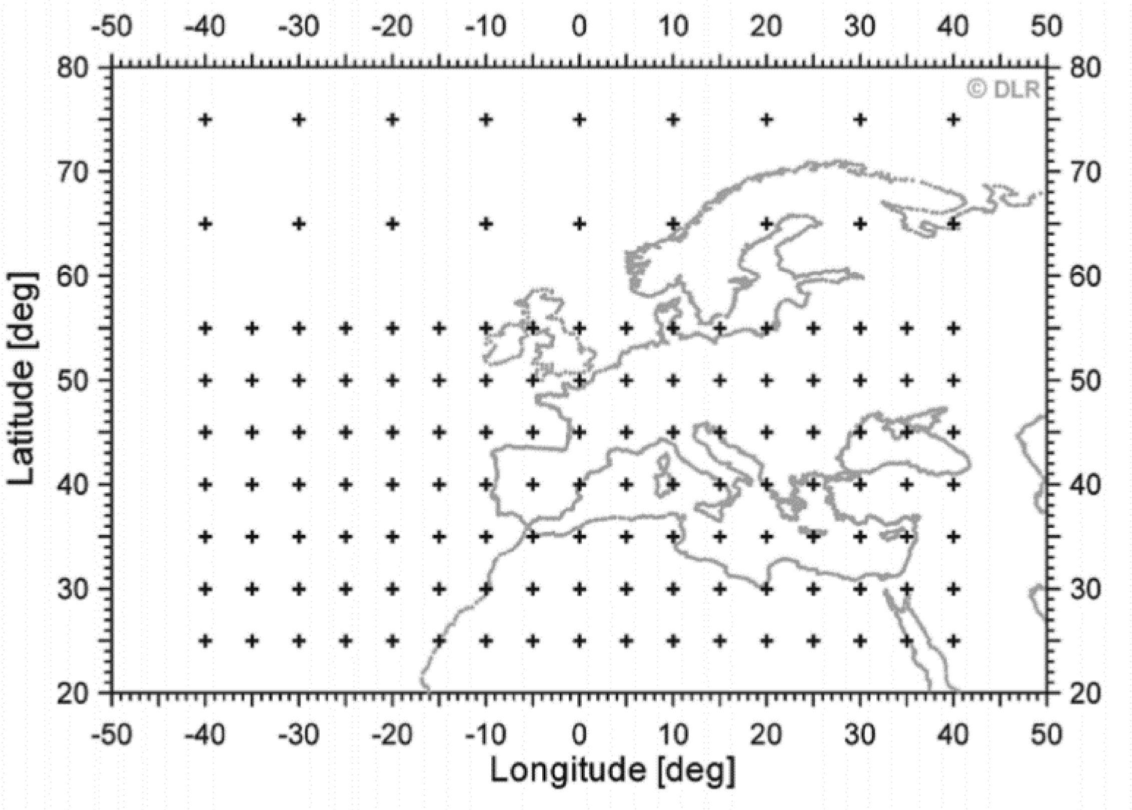

Figure 10, Ionospheric grid points of EGNOS [39].

The bounds for the residual errors in the ionospheric corrections are called grid ionospheric vertical errors (GIVEs). The GIVE bounds the ionospheric correction for a certain point in the grid for a line of sight that passes vertically through that point. Lines of sight of other angles get adjusted by a geometric obliquity factor to regulate the delay and confidence bounds of the longer ray path. Additionally, the master station also bounds the impact of satellite-specific errors after correction. These bounds are known as user differential range errors (UDREs) and bound the projection of the satellite clock and location errors to the worst-case location in the coverage area.

The final SBAS message which is broadcasted to the user via the GEOs contains ionospheric corrections, satellite specific corrections and associated bounds.

2.4.2 SBAS Architecture

The SBAS consists of the ground segment and the space segment:

- Ground segment
  - Reference stations
  - Master stations
  - Ground uplink stations
- Space segment
  - Geostationary satellites (GEO)

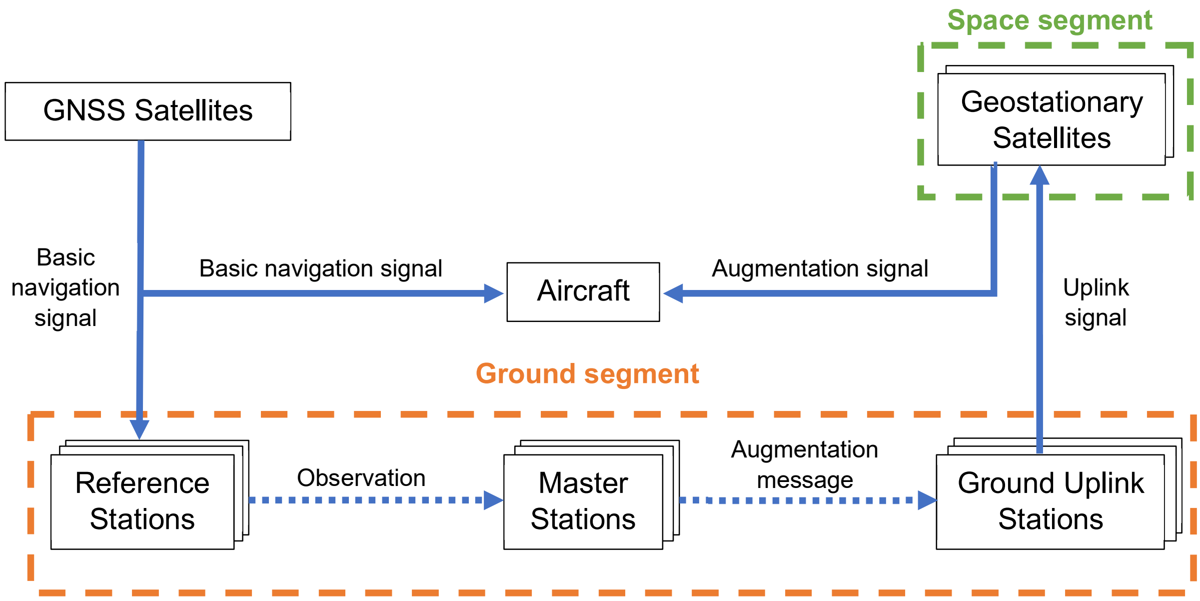

Figure 11, SBAS Architecture consisting of the Ground Segment and Space Segment and their interconnectedness with the GNSS satellites and the aircraft.

The ground segment consists of the reference stations, master stations and ground uplink stations. The reference stations collect the basic navigation data by the GNSS satellites in real-time and forwards this observation to the master station. There, integrity monitoring of the data is conducted, corrections are generated, GEO ranging is done, and this information is then compiled in the SIS augmentation message. This information is then forwarded to the ground uplink station, from where it is broadcast to users via the geostationary satellites of the space segment.

The following Figure 12 shows the ground segment of EGNOS, where reference stations are called Ranging Integrity Monitoring Stations (RIMS), master stations are called Mission Control Centres (MCC) and ground uplink stations are called Navigation Land Earth Stations (NLES). EGNOS consists of 40 RIMS, 2 MCC and 6 NLES (2 per GEO).

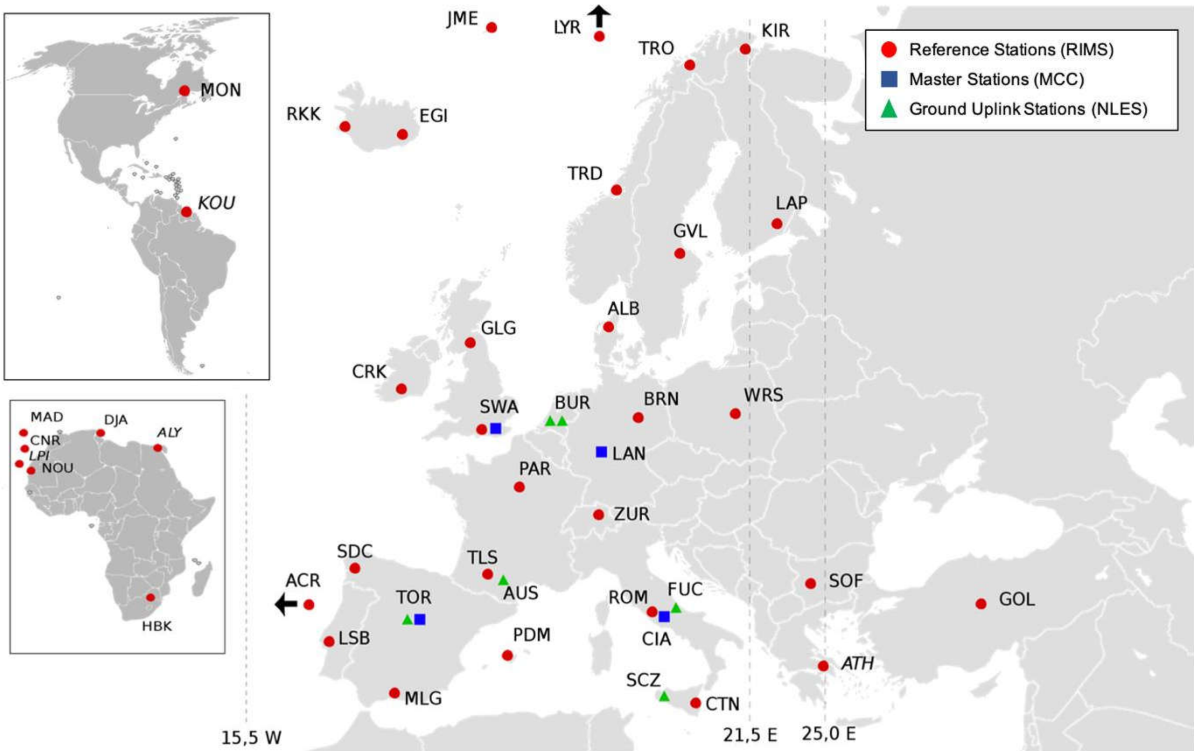

Figure 12, Ground Segment of EGNOS. Note that two additional facilities are given in the case of the two Master Stations, namely the Performance Assessment and Checkout Facility and the Application Specific Qualification Facility, which support system operations and service provision, Edited [40].

The following subsections describe the elements of an SBAS and elucidates on their functions and processes [40].

2.4.2.1 Reference Stations

A reference station consists of independent threads of reference equipment. Each thread contains an antenna, a dual-frequency GPS receiver, an atomic clock and redundant communication links. The redundant threads are included to guarantee any detection of hardware faults. Reference stations are located at facilities that can provide security, reliable power (with backup) and reliable communications equipment. The reference receivers take pseudorange and carrier-phase measurements every second and send these raw measurements to each master station along redundant communication lines. This means that solely data collection is done at the reference station, and the processing is done at the master stations.

2.4.2.2 Master Stations

Master stations collect the raw data sent by reference stations, formulate pseudorange corrections, determine confidence bounds and pack the information into messages for broadcast.

Every second, these stations receive raw information by every thread of every reference station. Firstly, the data undergoes a consistency check to identify and isolate erroneous data. The data of every parallel thread of a single reference stations must agree with each other and with previous information. The master station is able to identify and remove bad measurements before they are used downstream. The next step in the processing is the application of various filters and estimates of error sources on to the data. A satellite clock and orbit estimator that also estimates reference station clock offsets is applied. Also, safety monitors determine how much error may be present in the estimates. By screening measurements across multiple threads, most harmful errors are eliminated. Then, the monitors characterize the levels of code noise and multipath remaining on the measurements after error screening and carrier smoothing. It is very important to understand and bound the limits of observability, which is why these screened measurements are used to monitor errors on the satellites and estimated delays due to the ionosphere. The confidence values associated with each measurement are then propagated through the subsequent monitors to accurately find out how much certainty the monitors have in their ability to screen for errors.

The ionospheric delay is computed using dual frequency. The ionosphere is dispersive and so the ionospheric delay at L1 is different from the delay at L2. The observed delay is inversely proportional to the frequency squared, as seen in Equation (4) which means that with two equations at two different frequencies, it is possible to solve for the ionospheric TEC. Therefore, the SBAS ground system can estimate the ionospheric delay by taking advantage of this relationship.

The ionospheric delay value at each grid point is estimated from the individual ionospheric measurements from each reference station. Also, the GIVE bounds the ionospheric correction error at each grid point. The IGP are separated by roughly 500 km, which means that it is not possible to resolve a very fine scale structure of the ionosphere. This method for correcting the ionospheric delay therefore depends on the fact that the ionosphere is normally slowly varying over a region of several hundreds of kilometers. If the ionosphere happens to be in a more distributed state, the SBAS algorithm must recognize the problem and increase the confidence bounds accordingly.

The tropospheric delay is considered by a standard tropospheric model that predicts the amount of delay on both the reference station and user lines of sight. It is a verified climatological model based on years of observations that provides values for the barometric pressure, temperature, and other parameters given depending on the latitude and time of the year. This model also provides an upper bound on the error that may be remaining after the application of the model.

The satellite, ionospheric and tropospheric correction is applied to each reference station measurement to calculate the combined effect of the corrections for that specific line-of-sight. If the total error bound does not seem to properly bound all such measurements, the UDREs and GIVEs shall be increased. This range domain check is a further reasonability test to guarantee the consistency of the information. A final check is done by comparing the corrected position solution with the known surveyed location of its antenna. The range domain and position domain tests ensure that the corrections combine adequately and are independent. Therefore, a dependency of the errors with each other that leads to a magnification of the errors can be detected more easily since the errors in the position domain would become more obvious.

2.4.2.2.1 Master Station Correction Generation

The orbit and clock information are split into long-term and fast corrections. The long-term corrections are intended to correct for the slowly varying satellite orbit and clock errors, whereas fast corrections are designed to compensate for the rapidly changing part of satellite clock errors. Fast corrections are updated at a high rate (6 – 60 s), while long-term corrections are updated at a relatively low rate (120 s) [37] [41].

The fast term correction is computed as [42]

$$PRC_{i,fast} = PRC_{i,current} + RRC_{i,current} \cdot (t_{rec} - t_{i,current}) \tag{24}$$

Where $PRC_{i,current}$ is the closest matching PRC to the time of the observable (and within the timeout interval, which depends on the type of operation and the degradation factor), t_{rec} stands for the time of the observable, $t_{i,current}$ is the time of the $PRC_{i,current}$ and $RRC_{i,current}$ is the Range Rate Correction which is calculated as

$$RRC_{i,current} = \frac{(PRC_{i,current} - PRC_{i,previous})}{(t_{i,current} - t_{i,previous})} \tag{25}$$

where $PRC_{i,previous}$ is the PRC which matches the closest to the time of the $PRC_{i,current}$ within half of the timeout interval and $t_{i,previous}$ is the time of the $PRC_{i,previous}$. The other terms in Equation (25) are the same as in Equation (24).

Additional to the fast corrections, the long-term corrections are added, which consist of the correction factor IC_i for the ionosphere and the correction factor TC_i for the troposphere. The fast and long-term corrections are then added to the measured pseudodange after application of the satellite clock correction $PR_{i,measured}$. Therefore, the final total pseudorange correction equation is given as

$$PRC_i = PR_{i,measured} + PRC_{i,current} + RRC_{i,current} \cdot (t_{rec} - t_{i,current}) + TC_i + IC_i \tag{26}$$

2.4.2.3 Ground Uplink Stations and Geostationary Satellites

The Ground Uplink Stations (GUS) consist of several components:

- a computer to receive messages from the master stations
- an atomic clock to provide a stable frequency reference
- a signal generator to create the signal to uplink to the GEO
- a receiver to monitor the GEO downlink signal
- a GPS receiver to ensure the GEO is in sync to GPS time
- a controller to steer the uplinked signal.

Through the large footprint of a GEO on the earth, an SBAS can cover a large continental-scale region. The GEO signals are very similar to the GPS L1 C/A and L5 signals, respectively, on those frequencies. Since the signals are broadcasted from space, it is very unlikely that they are blocked by terrain in open sky environments where aircraft typically operate. The GEOs used for SBAS are basically simple transponders. They listen to analog signals at one frequency, translate it to the correct L-band frequency and transmit it toward Earth with minimum latency. The PRN code, messages and timing are all generated on the ground. The main use for the GEOs is the redirection of the signal from the GUS back toward the ground. The only change made by the GEOs is the conversion from the uplink frequency to the correct downlink frequency. This approach is due to the transponder payloads being lighter and less expensive than the full navigation payloads on GPS satellites. The GEO signals are generally less accurate than the GPS signals, due to the narrower bandwidth of the GEO's transponders. This difference creates a loss of precision and some signal distortion. By generating the signal on the ground, some of the uplink path errors due to the ionosphere or the troposphere cannot be fully removed and therefore affect the accuracy of the downlink signal. Also, since the GEOs move very slowly in the sky as seen from Earth, carrier smoothing does not reduce the multipath error on the ground at a static location. This leads to less accurate orbit and clock estimation and larger uncertainty in bounding the error. Motion of the aircraft causes enough variation so that carrier smoothing is effective in the aircraft.

2.4.2.4 Operational Control Centers

The Operational Control Centers are used to monitor the status and performance of an SBAS. The operators schedule maintenance and upgrades of various components at the reference, master and uplink stations. Additionally, weather, air traffic and traditional navigational aids are monitored. Interaction with other systems in the national airspace is ensured to guarantee a good integration of the SBAS. The control center is also used to produce notices to inform users of changes to the system performance and to interact with operators of GNSS.

2.4.3 SBAS Protection Level Computation

This chapter is according to [42]. Similar to GBAS, the integrity of SBAS is given through the PLs as explained in Chapter 2.2.2, Integrity. In case of a position error exceeding the PL for a longer time than the corresponding TTA during the certain operation, the user must be informed within the TTA, as seen in Table 2. The probability requirement defines that the overbounding of the position error for more than the corresponding TTA occurs no more than the corresponding continuity requirement as seen in Table 2 [37].

For the PL calculation, the error sources are approximated as a Gaussian distribution. The errors consist of four terms:

- Satellite clock and ephemeris errors (σ_{flt})
- Ionospheric delay errors (σ_{UIRE})
- Troposphere delay errors (σ_{tropo})
- Airborne receiver and multipath errors (σ_{air})

To get a conservative variance of the individual pseudorange error, the conservative variances of these single terms are combined [37].

$$\sigma_n^2 = \sigma_{flt,n}^2 + \sigma_{UIRE,n}^2 + \sigma_{tropo,n}^2 + \sigma_{air,n}^2 \tag{27}$$

The VPL is calculated as

$$VPL_{SBAS} = K_v \cdot d_U \tag{28}$$

where

$$d_U^2 = \sum_{n=1}^{N} s_{U,n}^2 \sigma_n^2 \tag{29}$$

Is the variance of model distribution that overbounds the true error distribution in the vertical axis. $s_{U,n}$ defines the partial derivative of the position error in the vertical direction with respect to the pseudorange error on the n-th satellite. Because the VPL is intended to bound 99.99999% of the errors, K_v is set equal to the Gaussian tail value of 5.33 [42].

Additional to the VPL, the HPL is calculated as

$$HPL_{SBAS} = K_H \cdot d_{major} \tag{30}$$

Where d_{major} corresponds to the error uncertainty along the semimajor axis of the error ellipse:

$$d_{major} = \sqrt{\frac{d_{east}^2 + d_{north}^2}{2} + \sqrt{\left(\frac{d_{east}^2 - d_{north}^2}{2}\right)^2 + d_{EN}^2}} \tag{31}$$

Furthermore,

$$d_{east/north}^2 = \sum_{n=1}^{N} s_{east/north}^2 \sigma_n^2 \tag{32}$$

is the variance of the model distribution that overbounds the error distribution in the east and north, respectively.

The term

$$d_{EN} = \sum_{n=1}^{N} s_{east,n} s_{north,n} \sigma_n^2 \tag{33}$$

describes the covariance of model distribution in the east and north axis.

The value of K_H for computing HPL is $K_{H,NPA} = 6.81$ for en route through non-precision approach, respectively $K_{H,PA} = 6.0$ for precision approach [42].

For precision approaches (weights w_i are equal to $1/\sigma_n^2$) the pseudorange variance is inverted and placed on the diagonal elements of the weighting matrix (W) and combined with the geometry matrix (G). Therefore, the covariance of the position estimate is formed as

$$(G^T W G)^{-1} \tag{34}$$

For a general least squares position solution, the projection matrix S is defined as in Equation (15.1). The reference frame in which the geometry matrix is expressed, is the local east, north up (ENU) frame.

3 Methodology

The methodological approach to answer the research questions, which are described in Chapter 1.2, Objectives of this Work, will be an analysis of quantitative data.

For this thesis, descriptive data of observations was gathered. This methodological approach was chosen since the research questions depend on the outcome of quantitative data. The integrity investigated in RQ1, as well as the accuracy investigated in RQ2 both can be measured quantitatively by analysing different values and discrepancies that occur in the data analysis. In this field of analysis, this is the standard methodological approach used to evaluate data. Valid research, as described in Chapter 2, Background, is required to generate a carefully designed study under controlled conditions that can be replicated by other researchers. The main criteria for the reliability of the study is a clear distinction between assumptions and facts. Therefore, if an occurring phenomenon in the data evaluation cannot be validated and backed by theory, it shall be characterized as an assumption based on the theoretical background. The main criteria for the validity of the study is to use the raw data, which is not modified in any way in order to prevent any biased results. Therefore, a reproduceable data evaluation can be achieved.

The method of data collection is conducted using quantitative methods. In September 2019, the DLR conducted experimental flight tests around Zurich Airport with the GBAS and SBAS-capable Airbus A320 “ATRA” research aircraft. “ATRA” stands for Advanced Technology Research Aircraft and is the DLR’s largest fleet member [43]. During the five-day flight test period, the aircraft was based in Dübendorf Air Base (LSMD) and conducted around 70 test flights at Zurich Airport. There, approach procedures were tested, and the raw receiver data (RINEX GPS observation and navigation files) was collected on board the aircraft. The reference data was collected by Skyguide or provided by the historical status services of the EGNOS ground infrastructure. The following data was collected:

Figure 13, Airbus A320 "ATRA" used for the flight test [43].

- RINEX GPS observation and navigation files (provided by the DLR)
- GBAS CAP files (provided by Skyguide)
- Carrier phase trajectory data (provided by Skyguide)
- RINEX B files with the historical SBAS messages as broadcast by the EGNOS GEO satellites (provided by EDAS)

The RINEX GPS observation and navigation files was provided for a time span of 2 hours (12:00 – 14:00 on the 10th of September 2019) and the GBAS CAP files were provided for a date range of 24 hours (00:00 – 23:59 on the 10th of September 2019). The carrier phase trajectory data and the EDAS RINEX B files were provided for a time span of 45 minutes (13:00 – 13:45 local time on the 10th of September 2019). To answer RQ1, this time span of 45 minutes (13:00 – 13:45 local time on the 10th of September 2019) is considered, since during this epoch the aircraft was performing precision approaches at LSZH and the respective reference trajectory data was available. During other epochs of the provided data, the aircraft was either positioning from or to LSMD. For RQ2, a time span of 24 hours (10th of September 2019) is evaluated, to prevent any biased results due to day dependencies in case a shorter time span is used. Here, static observations are investigated, which do not depend on the dynamic test flight data, but rather on the static data obtained through a receiver antenna on the ground.

Before the analysis, the gathered data was prepared. This was done using the PEGASUS program by EUROCONTROL, which is a standard program that focuses on this kind of data evaluation. Firstly, the information was checked for any missing data and if the correct file format is provided. Then, it was converted using the PEGASUS CONVERTER module to obtain the appropriate file format for the analysis. Finally, the final data sets, which were analysed in the data evaluation, were either obtained using the GNSS Solution Module or the Dynamics Module which are both modules of the PEGASUS program, which is explained in more detail in the Appendix. These final data sets were then visualized using Matlab, since this program offers a wide range of functions for adequately visualizing data. The final plots used in the data evaluation are flight path plots, horizontal position solution plots, histograms for vertical position solution, protection level plots, pseudorange correction plots, skyplots or Stanford-ESA integrity plots. Also, values such as standard deviations and correlations are calculated, and other parameters such as the NSV or the DOP are extracted using Matlab.

These methods allow for adequate data processing to obtain the most feasible results to answer the research questions in the data evaluation. Common plots used are the Stanford-ESA integrity plot or the skyplot allow for comparable and reproduceable results. Integration of several parameters in to one single plot allows for comparison of data that is interdependent or for illustration of correlations.

The limitation of the data valuation compared to other studies might be the investigation of a short time span. Also, only approach procedures at a single airport are investigated. To get a more broad and general comparison of the system performances, a cross-comparison of GBAS and SBAS considering several airports (and other SBAS like WAAS or GAGAN) including locations at the edge of an SBAS coverage, low latitudes with high ionospheric activity or comparisons between different solar cycle conditions could be conducted. Furthermore, certified standard equipment on board of a commercial aircraft could be used instead of the experimental equipment installed on board of the test aircraft used for the data evaluation.

4 Evaluation at Zurich Airport (LSZH)

In this section, the data evaluation at LSZH is discussed. Firstly, the test flight path is plotted, followed by a comparison of the GBAS, SBAS and standalone GPS position solution. Then, the integrity in terms of PLs for GBAS and SBAS are analysed and compared with the respective ALs. Also, an integrity diagram is created for SBAS and finally, the PRCs are plotted for GBAS and SBAS.

4.1 Test Flight Path

Figure 14 shows the flight path of the test aircraft during around 45 minutes of testing (13:00 – 13:45 local time). It shows multiple approaches into LSZH's runway 14 conducted from northwest with go arounds performed, followed by left turns back into northern direction to repeat the approach procedure. The location of LSZH is marked in red.

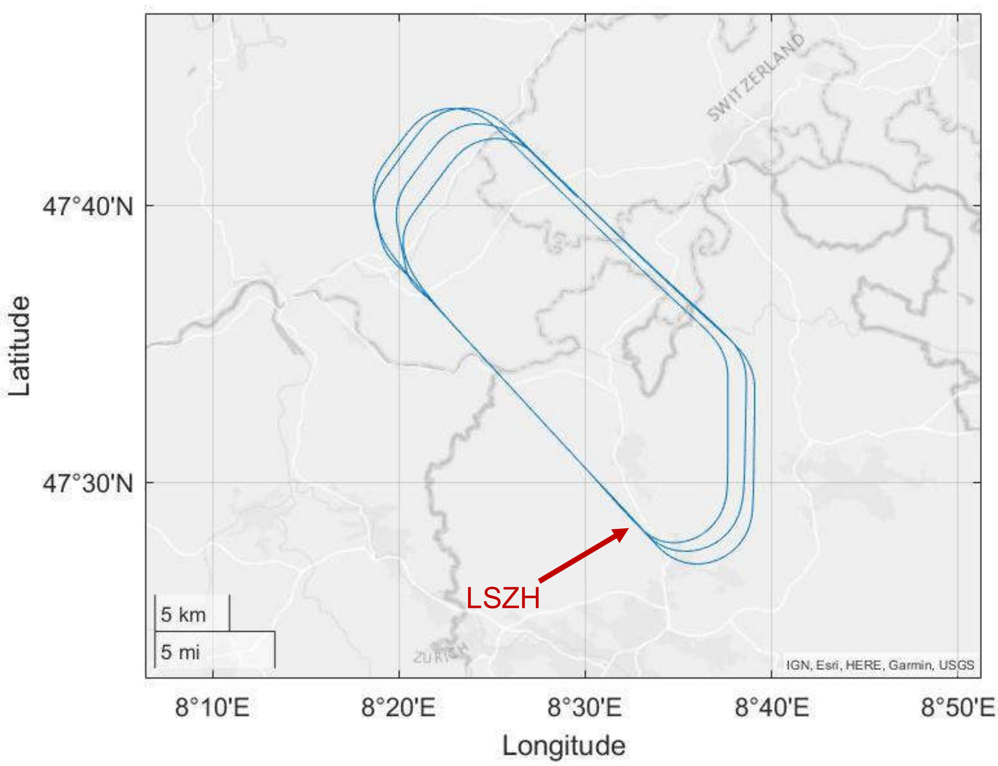

Figure 14, Flight Path of the test flight during around 45 minutes of testing.

4.2 Comparison of the GBAS, SBAS and standalone GPS position solution

In order to compare the accuracy of GBAS, SBAS and standalone GPS, a plot was created in which the position solutions of all three systems were calculated for the same static rover (RSMU #1 antenna at Zurich airport) over a whole day (September 10th, 2019), as seen in Figure 15. Each of the points represents a single position solution for the RSMU #1.

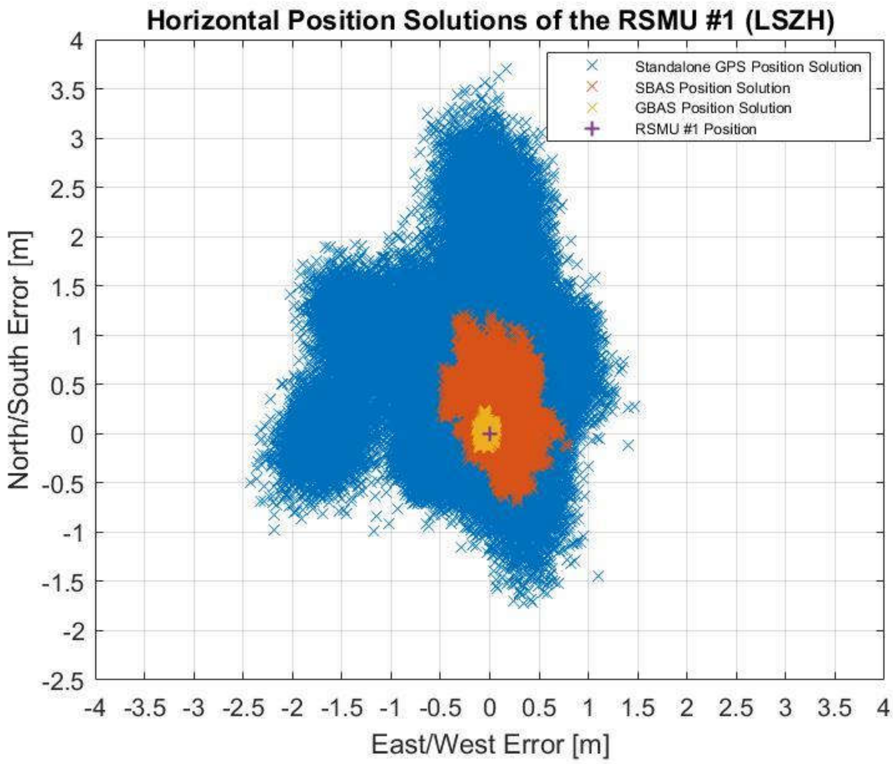

Figure 15, Horizontal position solution of the RSMU #1 antenna at LSZH calculated by standalone GPS (blue), SBAS (red) and GBAS (yellow) while the actual position of the RSMU #1 is located at (0, 0).

As expected, the standalone GPS position solution (blue) shows the largest inaccuracy compared to the two differential corrected position solutions of GBAS (yellow) and SBAS (red). Over the 24-hour timespan, the standard deviation of standalone GPS is 0.51 m in the horizontal plane and the largest outliers are in the range of 4 meters. These outliers are discussed in more detail in 4.3, Protection Levels for Integrity Investigation.

The SBAS corrected position solution accuracy lies between the GBAS and the standalone position solution. The standard deviation in the horizontal plane is around 0.19 m.

The GBAS corrected position solution is the most accurate of the three position solutions with the standard deviation being 0.025 m in the horizontal plane. Even the largest outliers are in a range of less than 0.25 m.

In Figure 16, the vertical plane is shown as a histogram. It is noticeable that the order of accuracy is the same as in the horizontal plane, but with larger standard deviations. The reason for this lies in the geometry of the satellites. The horizontal plane can be covered well by distributing the satellites from several elevations and azimuths in the sky above the rover. In the vertical plane this cannot be achieved, since an “optimal” coverage would require satellites from above and below the rover. However, this is not possible since no satellites can be placed below the rover.

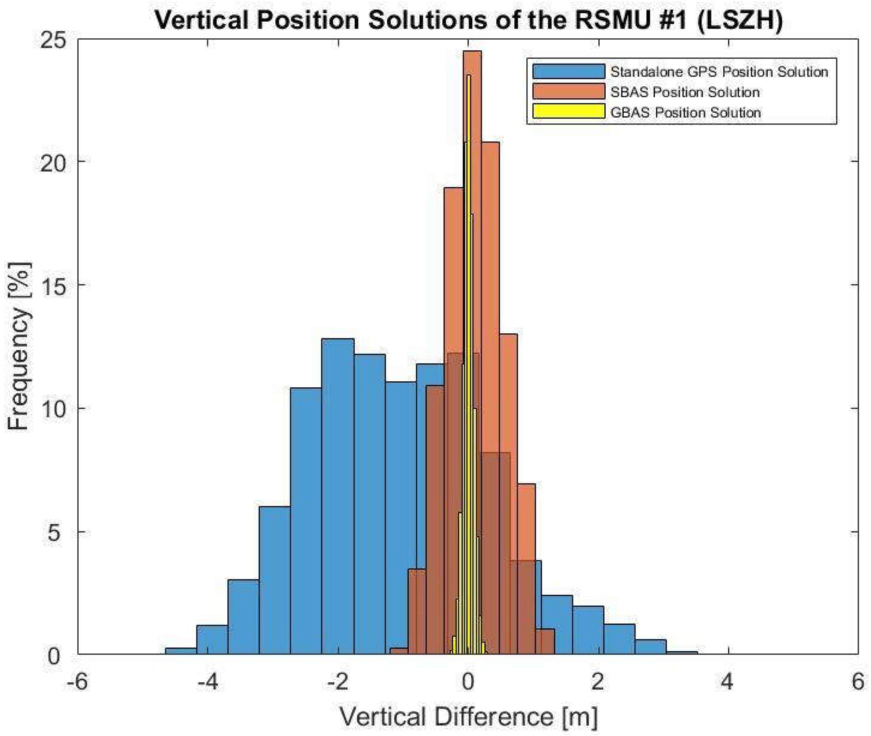

Figure 16, Histogram of the vertical difference of the calculated position solutions by standalone GPS (blue), SBAS (red) and GBAS (yellow) compared to the actual position of the RSMU #1 (LSZH) (vertical difference = 0).

The standard deviations in this case are 0.987 m for the standalone GPS position solution, 0.266 m for the SBAS corrected solution and 0.049 m for the GBAS corrected solution.

A summary of the standard deviations is given in Table 5:

Standard deviation:	Horizontal plane [m]	Vertical plane [m]
Standalone GPS	0.508	0.987
SBAS	0.186	0.266
GBAS	0.025	0.049

Table 5, Standard deviations of Standalone GPS, SBAS and GBAS in the horizontal and vertical plane.

To get a different view of the positional accuracy of standalone GPS and the associated GBAS and SBAS corrections and to see if there is a daily dependency, the vertical errors of the position solutions relative to the actual position of RSMU #1 were plotted against the time in Figure 17. This was done over a time span of 24 hours. Here it can be seen that the GBAS is able to keep its accuracy at roughly the same level throughout the day, while the SBAS and standalone GPS vertical errors show some variation. The standalone GPS vertical errors show greater variation compared to SBAS, and the errors mostly lie in the negative region. Overall, no daily dependency can be detected.

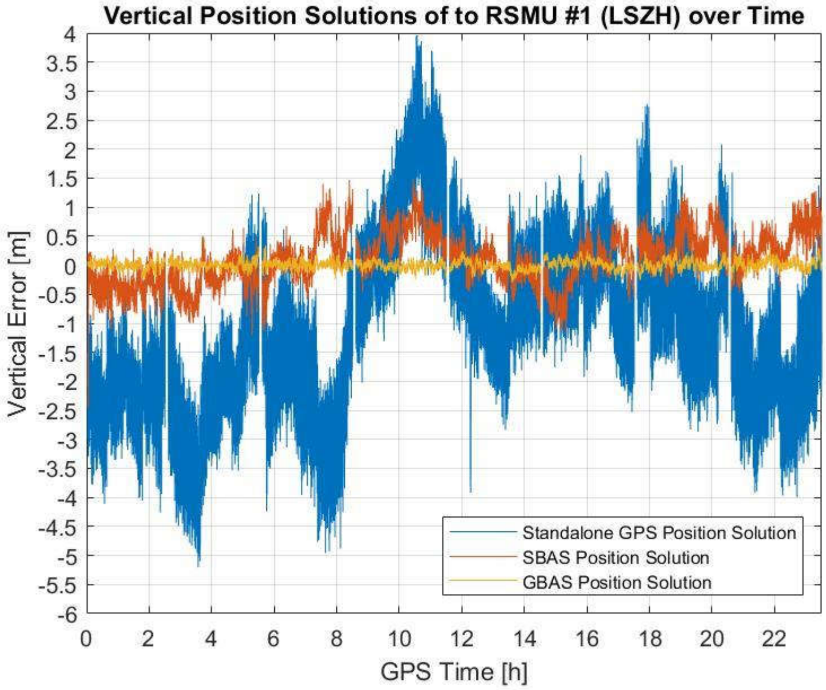

Figure 17, Vertical difference of the calculated position solution by standalone GPS (blue), SBAS (red) and GBAS (yellow) compared to the actual position of the RSMU #1 (vertical error = 0) over a full day.

4.3 Protection Levels for Integrity Investigation

As described in Chapter 2.2.2, Integrity, the PLs are an indicator for the performance, precisely the integrity, of a GBAS and SBAS corrected position solution. Basically, the higher the PLs, the lower the integrity of the calculated position solution. In Figure 18, the Vertical and Horizontal/Lateral PLs are plotted against the timeframe of the test period, once for GBAS and

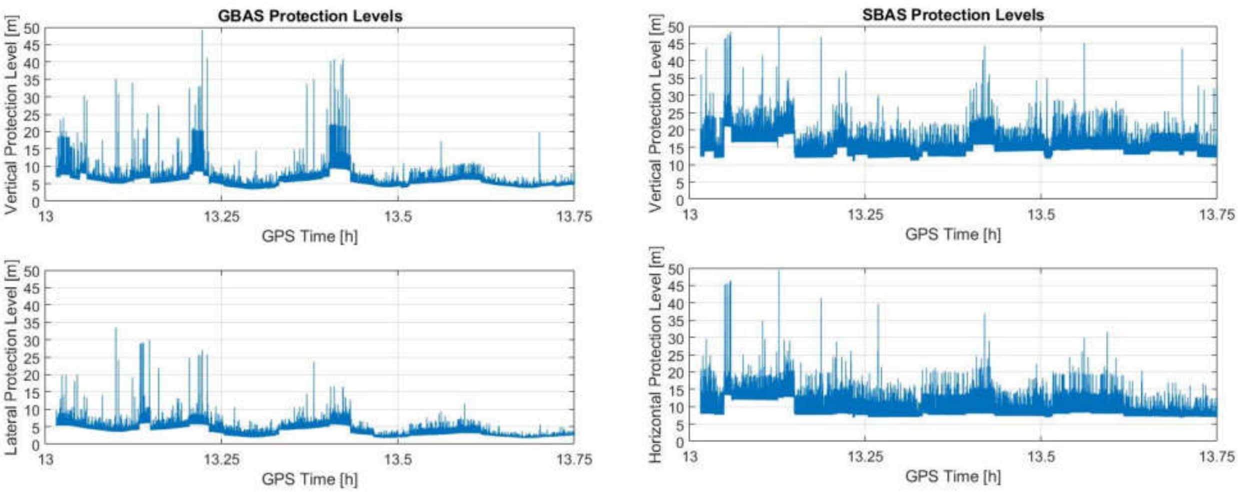

Figure 18, GBAS and SBAS Protection Levels for the test period (filtered to investigate the lower edges).

once for SBAS. Although the calculation of the HPL and LPL differ, they are used as a comparison for between GBAS and SBAS Pls in the horizontal plane. It is important to note that the PLs for both systems are filtered with a cut-off at 50 m. 10 out of 52904 values are filtered for GBAS and 14 out of 52904 values are filtered for SBAS. The reasons for such high peaks in the PLs are either due to initialization of the system, change in the approach procedure (from GBAS Precision Approach or SBAS Precision Approach to GBAS Non-Precision Approach or SBAS Non-Precision Approach, respectively) or due to weak satellite geometry combined with a low number of satellites used for the position solution. Through the filtering of the peaks, a more illustrative view of the lower edges of the PLs can be achieved.

It is visible that the values of the lower edge of the GBAS PLs are smaller, and there is less variation compared to the SBAS PLs. This is an indicator of a better PL-performance of the GBAS compared to SBAS. Both systems show vertical steps in the lower edges, and the lower edges of the GBAS PLs are not parallel to the x-axis, whereas the lower edges of the SBAS PLs are almost parallel to the x-axis.

The reason for the peaks in the PLs as seen in Figure 18 is that the number of satellites used usually drops to a lower value only for a single time stamp, which is mostly caused by a change in satellite geometry. Despite the number of satellites in direct line of sight as seen from the user mostly remains the same during such occasions, some satellites are being excluded for positioning. In all cases, the satellites are excluded from positioning due to the change in status flag of a satellite with regard to purely GNSS issues [44]. During the 45-minute test period, a total of 675824 times a GPS satellite was detected by the system (for GBAS and SBAS). Of those, 229189 times (33.9 %) a satellite was excluded from positioning for GBAS and 199082 times (29.5 %) a satellite was excluded from positioning for SBAS. The biggest reason for the exclusion of a satellite is the carrier phase smoothing filter not having settled, which accounted for 121524 exclusions (53.0 % of all exclusions of a satellite) for GBAS and for 121690 exclusions (61.1 % of all exclusions of a satellite) for SBAS. The other reasons for both systems excluding satellites from positioning are mostly due to other factors or a combination of other factors, such as no GPS/Galileo ephemeris data set available, GPS/Galileo ephemeris available, but selected set is unhealthy or timed out, satellite being below the selected elevation mask, gap between consecutive measurements too long and states must be initialized this epoch or satellite position not correct (comparison between almanac and ephemeris derived position).

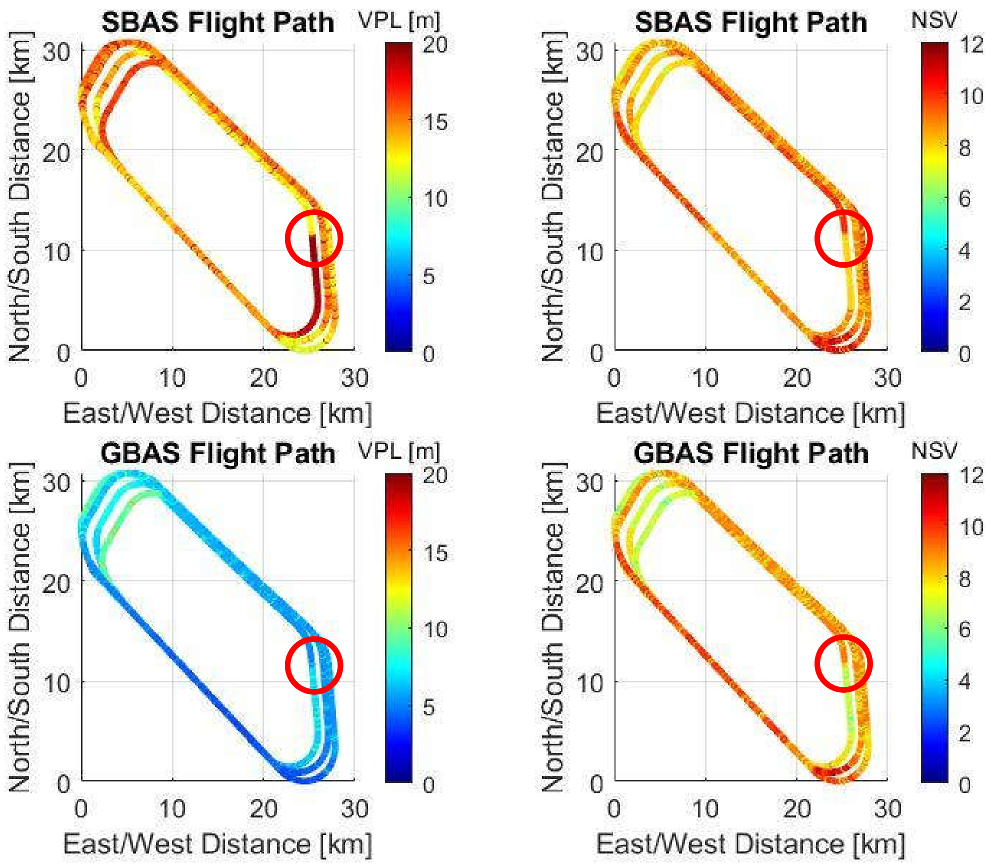

Figure 19, Vertical Protection Level and number of satellites used in dependence of the flight path.

Figure 19 shows the test flight path for the 45-minute time period for GBAS and SBAS, where the colour spectrum on the left plots marks the VPLs and on the right plots the number of satellites used (NSV). As also seen in Figure 19 the colour spectrum values of the PLs of GBAS are lower compared to the colour spectrum values of the PLs of SBAS.

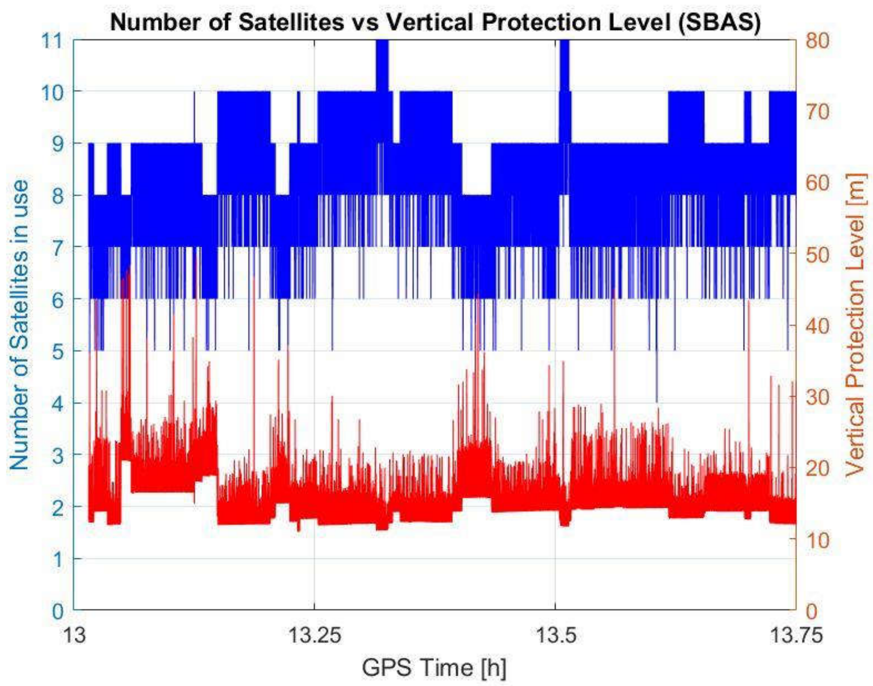

Figure 20, Number of satellites used with the Horizontal Protection Level during the test period.

Additionally, a relation between the PLs and NSV can be seen for both systems. An example for the relation is marked with a red circle, where, along the flight trajectory in northern direction, a sudden decrease in the PLs and a sudden increase in the NSV is visible for both systems. Therefore, as discussed in Chapter 2.1.4.4, Satellite Geometry it can be said that the more satellites are used for the position solution, the lower the PLs and thus the better the integrity of an augmentation system. This correlation can also be confirmed by plotting the NSV and the PLs during the timeframe of the flight test, as seen in Figure 20. In this case, SBAS NSV and VPL is used for demonstration purposes, although the correlation is also visible for SBAS HPL and for GBAS VPL and HPL. By comparing the lower edge of the PLs (red) with the upper edge of the NSV (blue), a trend can be seen, where generally the more satellites used, the lower the PLs. In Figure 20, the correlation between NSV and PLs is -0.8007.

In addition to the correlation between the PLs and the NSVs, Figure 19 shows that the PLs are above average (compared to the investigated 45-minute test period) for a longer period. The PLs then decrease to average values (compared to the investigated 45-minute test period) when the graph turns yellow between position 5 and 5. To investigate this in more detail, this area was plotted again at a higher resolution in Figure 21.

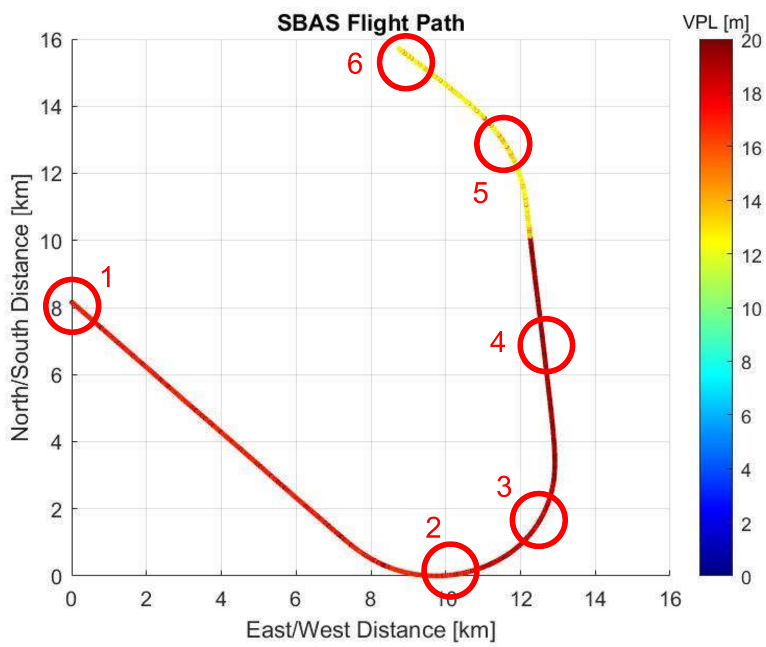

Figure 21, Section of the Vertical Protection Level in dependence of the flight path.

The red area in Figure 21 has a mean value of 8.7 for the NSV. This corresponds to a reasonable value but still the PLs are relatively high in a range of 16 to 20 m. Although the NSV has a large impact on the position solution accuracy, the geometry of the used satellites is also crucial.

To find an explanation for these relatively high PLs, the satellite geometries were plotted in a skyplot for the respective marked flight path locations 1-6 circled in red in Figure 21.

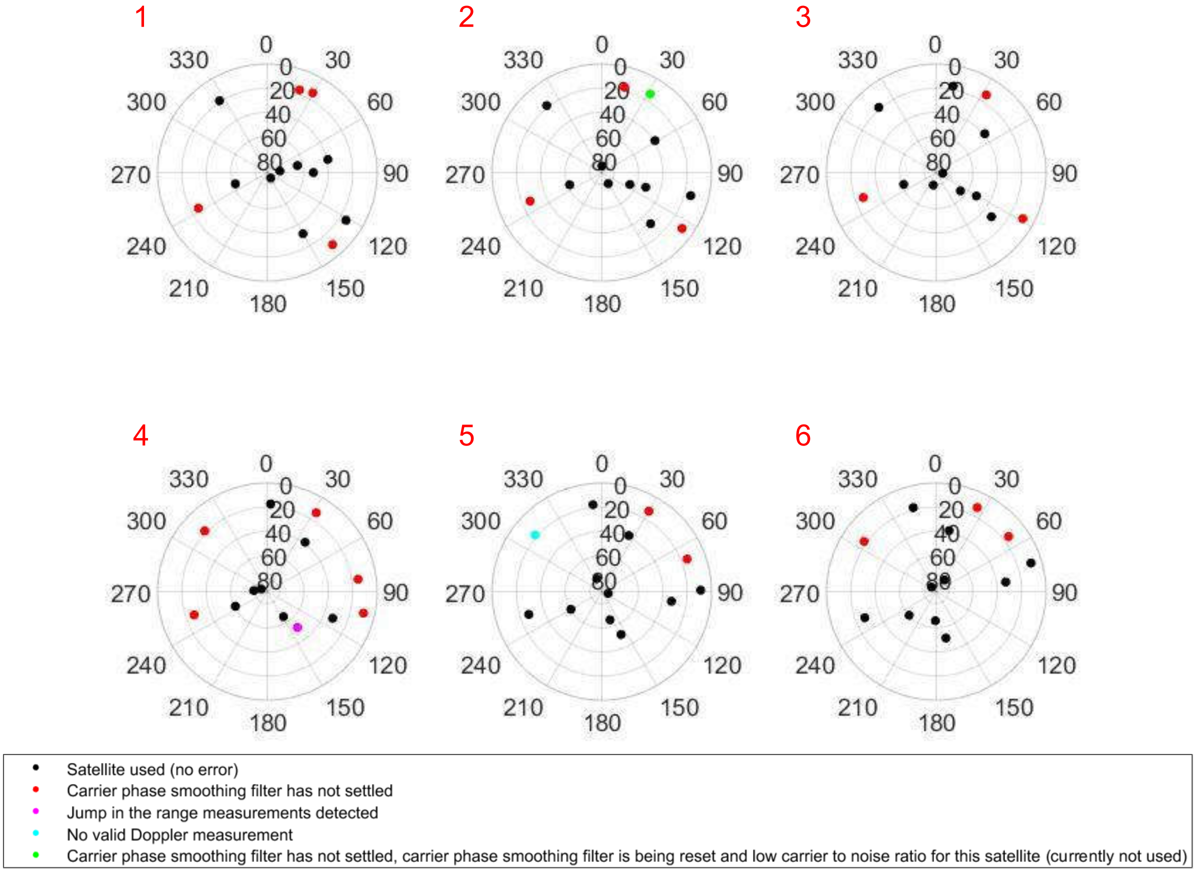

Figure 22, Skyplots with the used and excluded satellites for position 1-6 of the investigated flight path section.

The satellite conditions are marked by colour in Figure 22. As described in Chapter 2.1.4.4, Satellite Geometry, the DOP value can be used to get a theoretical indicator for the expected position accuracy. The HDOP, VDOP and TDOP values can be found for all positions in Table 6.

Position	Horizontal DOP	Vertical DOP	Total DOP
1	1.49237	1.93198	1.58781
2	1.492	1.94284	1.59584
3	1.66575	2.36956	1.93124
4	2.03569	2.87456	2.45819
5	1.06285	1.43145	1.06318
6	1.06098	1.43398	1.06353

Table 6, Horizontal, vertical, and total dilution of precision values for position 1-6 of the investigated flight path section.

In position 1 the VPL is approximately 16 m with 9 satellites being used, and another 4 satellites being in visual contact but excluded for the position solution. This is most likely since 6 of the 9 satellites are in a line extending from about 80 degrees to 260 degrees. Therefore, the coverage is not optimal, and the VPL is accordingly high. For this time point, the VDOP is relatively high and thus the expected position solution accuracy is low.

In position 2, the aircraft is at the turn entry, which changes the bank angle of the aircraft and thus the satellite geometry relative to the aircraft. Here, the change in bank angle is still small and therefore the PLs and DOP values remain in a similar range.

In position 3, the aircraft is banked due to the curved flight path, with the maximum bank angle reached. At this point the relative geometry to the aircraft also changes significantly. There are still 9 satellites used, but a certain pattern occurs where most of the satellites are in a line, which is rather disadvantageous for the HDOP. Thus, the geometry in this state is unfavourable. This is also confirmed by the DOP values as they increased by 17.4% in total compared to position 2. This might also be an explanation why the VPL rises to about 18-20 m for this flight path location.

In position 4, the aircraft is flying in a straight line again but with a different heading. Similar to position 2, the change of the bank angle leads to a change in the satellite geometry relative to the aircraft. But what happens primarily is a reduction in the number of satellites used (from 9 to 7 satellites). As a result, the PLs increase. The DOP value also increases here, specifically the VDOP increases to 2.87 which is an increase of 67 % compared to the VDOP of position 1.

In position 5 and 6 the VPL decrease again to about 12-13 m. Through the corresponding skyplot, it is noticeable that the number of satellites used increases to 10 and the geometry shows better distributions. Nevertheless, some satellites still obscure each other which is also confirmed by the DOP value. The TDOP is 1.064 and the VDOP is 1.434.

This example shows a correlation between the DOP and the PLs and that satellite geometry has a significant influence on the PLs.

4.4 Protection Levels vs. Alert Limits

As seen in Chapter 2.2.4, Availability, the availability is given, when the PL values remain smaller than the AL values during 99% to 99.999% of the time. Like the comparison made for the HPL and LPL, for the context of this work the LAL and HAL are used as a means of comparison for GBAS and SBAS. Also, compared to Figure 19, the PLs are not filtered with a cut-off at 50 m.

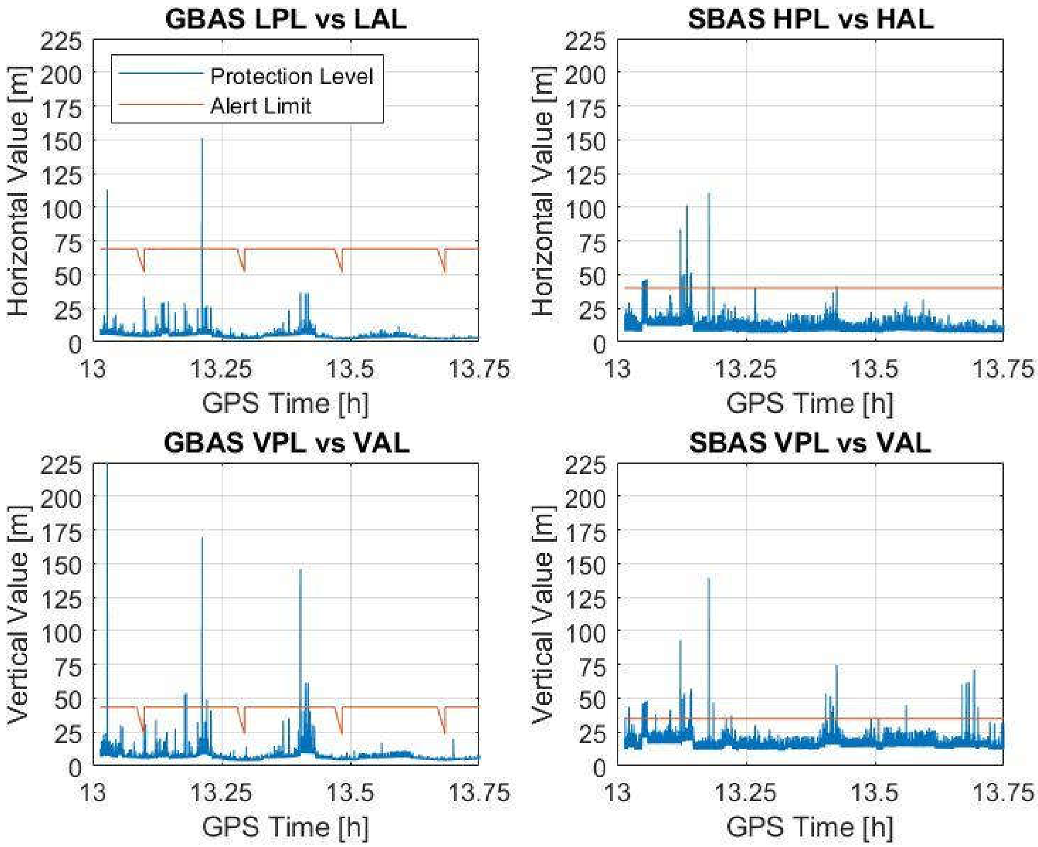

Figure 23, GBAS and SBAS Protection Levels and Alert Limits for the test period.

As seen in Figure 23, for GBAS the LPL exceeded the LAL twice and the VPL exceeded the VAL ten times during the 45-minute test period. For SBAS, the HPL exceeded the HAL 15 times and the VPL exceeded the VAL 36 times.

The reason for the ALs not remaining constant in the case of GBAS is the different requirement for ALs for different operations, as seen in Table 4. The four incisions in the GBAS ALs represent the aircraft's final approach phase, where the ALs decrease due to the aircraft's change in relative position to the GBAS ground station.

In the case of GBAS, 2 out of 52904 LPL computations for this certain test period are above the LAL, thus indicating an availability of 99.99 %. For the VPL, 10 out of 52904 VPL computations for this certain test period are above the VAL, therefore indicating an availability of 99.98 %. In the case of SBAS the HPL, 15 out of 52904 HPL computations for this certain test period are above the HAL, therefore indicating an availability of 99.97 %. For the VPL, 36 out of 52904 VPL computations for this certain test period are above the VAL, therefore indicating an availability of 99.93 %. Since both the availability in the horizontal and vertical plane are necessary to provide the service, only the lower value of both components is used to determine the availability of a system. Therefore, the availability during the 45-minute test period is 99.98 % for GBAS and 99.93 % for SBAS.

If the LPL/HPL or VPL exceed the LAL/HAL or VAL, respectively, no actions in terms of warnings sent to the primary flight display or flight computer are taken, as long as the excess is no longer than the TTA at this current type of operation, as described in Table 2. Since, during this test period, no exceeding lasts longer than the TTA during the type of operation at this moment, the pilot does not receive any warnings, but rather notices a gap in the guidance provision during the exceeding.

To visualize the situation from a different perspective, in Figure 24 a Stanford-ESA integrity diagram was plotted for the SBAS scenario. The Stanford-ESA integrity diagram allows observations about the system performance of SBAS, highlighting the integrity margins. This is a standard methodology for the investigation of SBAS Integrity. A reference trajectory is required to generate a Stanford-ESA integrity diagram. In this case it is the carrier phase trajectory data that is provided by Skyguide. The carrier trajectory is extremely close to the true location of the aircraft, which is why this is suitable to assess the positional error calculated by the SBAS in reference to the true position. Therefore, the Vertical Position Error (VPE) can be calculated as the vertical difference between the SBAS position solution and the carrier phase position solution.

The Stanford-ESA integrity diagram allows to distinguish between two different types of integrity events [45] [46]:

- Misleading Information (MI): Event occurs when the system declared available, the position error exceeds the protection level but not the alert limit
- Hazardously misleading information (HMI): Event occurs if the system is declared as available, the position error exceeds the alert limit

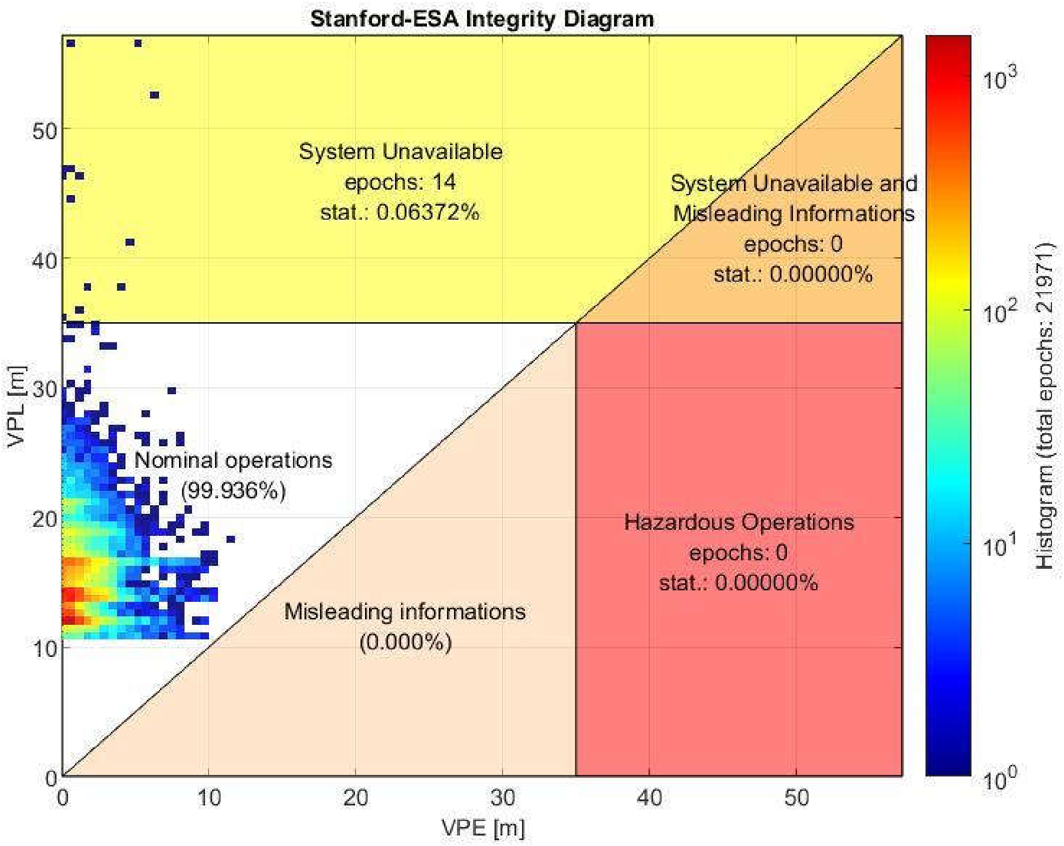

Figure 24, Stanford-ESA Integrity Diagram for the 45-minute test period (SBAS).

The vertical position error (VPE) is plotted on the x-axis and the VPL on the y-axis. At 35 m, the VAL for LPV-200 (as seen in Table 4) is plotted for both the VPE and the VPL. The system shows an availability of 99.936% (Nominal operations). In 14 out of 21971 epochs, the system is unavailable which corresponds to 0.06372%. This meets the availability requirement for SBAS as given in Table 2. In the entire flight phase analysed, no misleading information was discovered, and the integrity was always provided due to the protection levels bounding the position error.

4.5 Pseudorange Corrections (PRC)

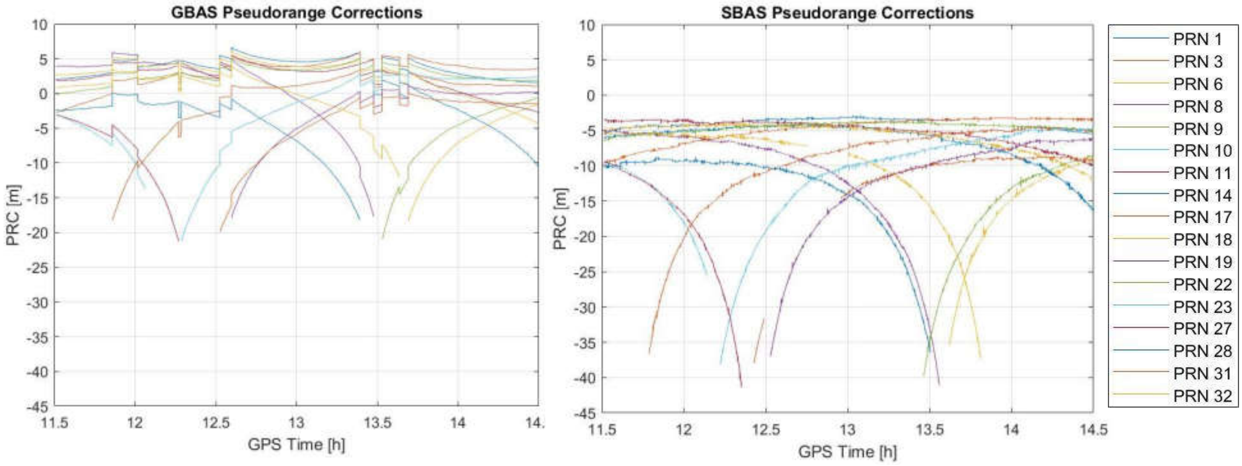

Figure 25, GBAS and SBAS pseudorange corrections for the used satellites during the test period.

Figure 25 shows the pseudorange corrections in meters generated by the GBAS (left figure) and the SBAS (right figure) over a 3-hour period for the GBAS RSMU #1 position solution at LSZH. Each colour represents one of the satellites used during this time period.

The plots show that both GBAS and SBAS provide pseudorange corrections, and both consider the elevation angle of the satellites. This is visible through the individual lines, where the PRC for a single satellite increases and decreases over time, which is due to the change of the satellite elevation relative to the user. The smaller the satellite elevation relative to the user, the longer the distance through the atmosphere. Therefore, due to the bigger impact of the ionospheric and tropospheric delay, the value of the respective PRC of this satellite increases.

Although the PRC's for the SBAS are shifted along the y-axis compared to the PRC's of GBAS, this difference in the y-axis values has no influence. Therefore, the pseudorange corrections of the GBAS or the SBAS could be shifted arbitrarily far on the y-axis, without influencing the final position solution. The reason is that this shift of the PRC's is simply compensated by the user clock error b_u from Equation (1).

On the plot with the PRC's for the GBAS, steps are visible that run vertically through all the satellite graphs. The reason for this can be explained by using Equation (7), respectively with the calculation of the PRC's (see Chapter 2.3.1.1.1, Ground Subsystem Correction Generation). The GBAS gives a weighting w_j to each satellite which is used for the position determination. If a new satellite is added or one is dropped (e.g. elevation <5°), then this weighting w_j is changed instantaneously and thus the PRC changes as well. Therefore, the GBAS considers the weight of every single satellite and geometry changes have an influence on the PRC's, since the PRC's are interdependent.

With the SBAS, the calculation of the PRC's looks different compared to GBAS, as seen in Chapter 2.4.2.2.1, Master Station Correction Generation. There are no individual weightings and therefore these vertical steps in the PRC's do not exist. The SBAS makes general corrections, which can be applied to a much larger area, but which are also less accurate than the PRC's generated by the GBAS, which can be seen based on the position solutions of GBAS and SBAS in Chapter 4.2, Comparison of the GBAS, SBAS and standalone GPS position solution. The SBAS includes all visible satellites for the calculation of the PRC's permanently (if there is no error) and applies the same weight to each satellite. Therefore, compared to the case of GBAS, the PRC's of SBAS are independent from one another.

5 Discussion

This work was performed to analyse the future potential of GBAS and SBAS based on the current performance of both augmentation systems. The analysis focused on a comparison of the accuracy and the integrity performance of both systems, which was conducted by investigating flight tests using commercially operational GBAS and SBAS approach procedures.

The results in terms of position solution accuracy of the static scenario indicate that the GBAS shows a better performance compared to SBAS (Research Question 2). It is important to note that the absolute values of the position solution error relative to the static reference position is a fraction of the requirements for CAT-I/LPV-200 precision approaches (see Table 3). This seems very optimistic but might be a result of the great RSMU #1 performance, which has minimized disturbances by error sources such as multipath. Therefore, the accuracy of dynamic position solutions during a flight might be less, also due to the experimental equipment installed on the test aircraft. GBAS and SBAS greatly increase the position solution accuracy compared to standalone GPS. This is illustrated visually with the use of plots, as well as numerically by the comparison of the standard deviations of the position solution of each system relative to a static receiver.

In terms of integrity, the protection level performance of GBAS is better compared to the protection level performance of SBAS (Research Question 1). It is important to note that for this work, the analysis in the horizontal plane was done by directly comparing the LPL with the HPL. The GBAS protection levels show less variation compared to the SBAS protection levels and generally, the values of the lower edge, as discussed in Chapter 4.3, Protection Levels for Integrity Investigation, are smaller for GBAS than for SBAS. Also, the lower edges of the GBAS protection levels show the dependency of the GBAS protection level computation on the distance to the GBAS ground station and the altitude above the ground of the airborne user. In the case of SBAS, the lower edges are almost parallel to the x-axis due to the system not depending on the user's relative distance to the threshold.

The results support the fact that the protection levels strongly depend on the satellite geometry and the number of satellites in use. Correlations can be identified between the NSV and the PLs, as well as the HDOP/VOP and the PLs. The reason for the protection levels exceeding the alert limits at times is mostly due to sudden changes in satellite geometry. Most of the time this happens in turns where the antenna points away from the satellites and low elevation satellites are shadowed by the fuselage and/or wings which results in a loss of tracking of the satellites. However, it also occurs during a straight flight where satellites are momentarily excluded due to other errors, such as carrier phase smoothing filter not settled or being reset, jumps in the range measurements detected, invalid doppler measurements or low carrier to noise ratio for a certain satellite.

In the investigated flight, the availability of GBAS is 99.98 % (99.99 % in the lateral and 99.98 % in the vertical plane), whereas the availability of SBAS is 99.93 % (99.97 % in the horizontal and 99.93 % in the vertical plane). This shows a slightly better availability for the GBAS, although both systems are well within the range of the availability performance requirements. It is important to note, that in this work, the availability was only evaluated during a 45-minute time span and in a flight pattern that was significantly more dynamic including several go-around manoeuvres than an average flight from an origin to a destination. Therefore, these values do not necessarily represent the true availability of both systems during regular operations.

Due to the PRCs it can be observed that averaging each single satellite has an influence on all other satellites, whereas the PRCs for SBAS are independent from one another. Due to the weighting of the individual satellites in the GBAS PRC computation, the PRC's shift with each geometry change, which is visible in the PRC plot through the steps. On the other hand, the PRCs of SBAS show a smooth change over time, where no sudden steps are visible due to the equal weight given to each PRN. As expected, the satellite elevation shows a dependency on the PRCs due to the influence of the ionospheric and tropospheric delay. The PRCs are at their highest relative value for the lowest satellite elevations and at their lowest relative value for the highest satellite elevations.

The generalizability of the results can be seen as limited by the fact that the DOP values used for the evaluation of the dependency of the satellite geometry on the protection level computation are only a theoretical, rather than a practical indicator. In practice, the important values used to determine the influence of the satellite geometry on the performance remain the $s_{vert,i}$ and $s_{lat,i}$ values for GBAS and the $s_{U,i}$ values for SBAS as described in Chapters 2.3.2, GBAS Protection Level Computation and 2.4.3, SBAS Protection Level Computation. These values describe the weight, that is given to each satellite, therefore influencing the impact of each satellite on the actual satellite geometry. Also, the reliability of the results is limited due to the test flights being conducted using experimental antennas on the test aircraft and only considering a short time span compared to previous research done on GBAS and SBAS. The latter can be justified by the objective of this work being a comparison between systems, rather than a full performance evaluation of each system over the long-term.

Generally, it can be said that although both systems' performances are satisfactory relative to the performance requirements, GBAS offers higher overall performance compared to SBAS in terms of PLs and accuracy. Furthermore, the availability of GBAS is slightly better for the 45-minutes test period.

5.1 Conclusion and Outlook

This chapter summarizes the work done to answer the research questions of this thesis and provides an outlook on the future of GBAS and SBAS and further research questions that could be answered in further development of the current work.

Firstly, the necessary theoretical background was covered to understand the fundamental concept of the research questions. This knowledge was then used to evaluate the data of test flights at LSZH, where the integrity performance in terms of PLs (RQ1) and performance in terms of position solution accuracy (RQ2) has been analysed. The Analysis was done by comparing the named parameters for GBAS and SBAS to answer RQ1 and for GBAS, SBAS and standalone GPS to answer RQ2.

The results show that GBAS achieves the best performance compared to SBAS and standalone GPS in terms of accuracy of the position solution. Furthermore, GBAS provides better integrity performance compared to SBAS, making it the ideal succession for ILS CAT-II and CAT-III precision approaches. However, the performance of GBAS CAT-III is slightly worse due to the shorter smoothing time constant in the carrier smoothing filter resulting in slightly increased residual noise and multipath residuals in the position solution. With the certification of already existing, improved GBAS approach guidance procedures for civil aviation, it is possible to use the full potential of GBAS in the future. This potential includes increased and variable glide slope angles for noise abatement, multiple glide slope angles for wake vortex mitigation and therefore less spacing of aircraft on the approach, multiple runway aiming points to optimize separation and minimize runway occupancy and taxi times to ultimately increase the capacity of a runway and vertical guidance of curved approaches. These variable operations are possible thanks to the flexibility to define reference paths for aircraft by waypoints, straight and curved segments and vertical profiles, whereas the ILS is only capable of straight-in approaches due to its physical limitation. Although, the current GBAS state of the art with straight-in CAT-I approach guidance does not provide any significant advantages over the ILS yet. The ultimate of GBAS is the support of automated taxi operations and precision departure guidance. Currently, GBAS CAT-I precision approach guidance does not bring any operational benefits in the SBAS coverage area, since the current SBAS state of the art already provides enough performance for such operations with less operational effort. GBAS is ideal for implementation at large airports with multiple runways and operating concepts, whereas SBAS implementation is significantly cheaper as it does not require ground installations. Hence, SBAS is more economically attractive for smaller regional airports with few runways and few operating concepts. Also, the large coverage area of SBAS allows services for locations currently not served by other navigation aids. EGNOS is set to evolve with major evolution by 2025 by the introduction of EGNOS V3, where expansion to dual-frequency and multi constellation including Galileo is planned to be implemented [47]. These expansions can improve the accuracy and reliability of the positioning, navigation and timing information over Europe [48].

New research questions that focus on the availability and continuity RNP's or the further dual-frequency and multi constellation implementation of both systems for civil aviation can expand the current thesis. Also, GBAS CAT-III performance could be evaluated and compared with current ILS CAT-III performance. Additionally, a comparison of the GBAS and SBAS including locations at the edge of an SBAS coverage, low latitudes with high ionospheric activity or comparisons between different solar cycle conditions could be conducted. Furthermore, the performance of different aircraft types and approach procedures could be analysed. The examination of such scenarios may allow a broader evaluation of both system's performances in different use cases. Also, due to the gained knowledge about the different operational advantages and disadvantages of GBAS and SBAS, an assessment evaluating at which local or regional environments it makes sense to introduce either GBAS or SBAS procedures could be conducted. These local or regional environments might differ in terms of airspace capacity, surrounding terrain, operating aircraft types, occurring weather conditions, noise abatement requirements, economic benefits and therefore call for either implementation of GBAS or SBAS procedures. As a final proposal, certified standard equipment on board of a commercial aircraft can be used instead of the experimental equipment installed on board of the test aircraft used for the data evaluation.

Bibliography

[1] International Civil Aviation Organization (ICAO), ‘Future of Aviation’. [Online]. Available: https://www.icao.int/Meetings/FutureOfAviation/Pages/default.aspx. [Accessed: 05-Mar-2021]

[2] Interoperability Working Group (IWG), ‘Global SBAS Status’, Feb-2020.

[3] R. Guillet, ‘Concept and benefits of GBAS - SBAS’, 06-Mar-2019.

[4] GMV, ‘GNSS Augmentation - Navipedia’, 2011. [Online]. Available: https://gssc.esa.int/navipedia/index.php/GNSS_Augmentation. [Accessed: 05-Apr-2021]

[5] EDAS, ‘EDAS DGNSS Coverage Map | EGNOS User Support’. [Online]. Available: https://egnos-user-support.essp-sas.eu/new_egnos_ops/resources-tools/edas-dgnss-coverage-map. [Accessed: 05-May-2021]

[6] APAC Office - ICAO, ‘Implementing ground-based and satellite-based augmentation systems’, *Uniting Aviation*, 02-Jul-2019. [Online]. Available: https://unitingaviation.com/regions/workshop-implementing-gbas-sbas/. [Accessed: 05-May-2021]

[7] Federal Aviation Administration, ‘Satellite Navigation - GBAS - How It Works’, 21-Nov-2016. [Online]. Available: https://www.faa.gov/about/office_org/headquarters_offices/ato/service_units/techops/navservices/gnss/laas/howitworks/. [Accessed: 06-Mar-2021]

[8] Jeppesen Sanderson, ‘Approach Charts LSZH’. 2006.

[9] ‘Neue Flugverfahren’. [Online]. Available: https://www.flughafen-zuerich.ch/unternehmen/medien/aktuelle-themen/neue-flugverfahren. [Accessed: 06-Jun-2021]

[10] M. Felux, ‘Gastvortrag GNSS, unpublished’, Zurich, ZHAW SoE, 2019.

[11] EDAS, ‘LPV PROCEDURES MAP | EGNOS User Support’. [Online]. Available: https://egnos-user-support.essp-sas.eu/new_egnos_ops/resources-tools/lpv-procedures-map. [Accessed: 21-May-2021]

[12] ‘Swiss hat ihren Nachzügler-A220 bekommen’, *aeroTELEGRAPH*, 25-May-2021. [Online]. Available: https://www.aerotelegraph.com/swiss-hat-ihren-nachzuegler-a220-bekommen. [Accessed: 04-Mar-2021]

[13] C. J. Hegarty and E. Chatre, ‘Evolution of the Global Navigation Satellite System (GNSS)’, vol. 96, no. 12, pp. 1902–1917, Dec. 2008.

[14] EDAS, ‘About EGNOS | EGNOS User Support’. [Online]. Available: https://egnos-user-support.essp-sas.eu/new_egnos_ops/egnos-system/about-egnos. [Accessed: 20-Apr-2021]

[15] EUSPA, ‘Aviation’. [Online]. Available: https://www.euspa.europa.eu/segment/aviation. [Accessed: 25-Mar-2021]

[16] ESA, ‘Satellite frequency bands’. [Online]. Available: https://www.esa.int/Applications/Telecommunications_Integrated_Applications/Satellite_frequency_bands. [Accessed: 03-Mar-2021]

[17] J. Sanz Subirana, J. Z. JM, and H.-P. M, ‘GNSS signal - Navipedia’, 2011. [Online]. Available: https://gssc.esa.int/navipedia/index.php/GNSS_signal. [Accessed: 18-Mar-2021]

[18] HEXAGON, ‘GNSS Frequencies and Signals’. [Online]. Available: https://novatel.com/support/known-solutions/gnss-frequencies-and-signals. [Accessed: 03-Apr-2021]

[19] C. Mihaela-Simona, F. Michael, C. Maria, and Daniel Gerbeth, ‘The Ground Based Augmentation System for Civil Aviation: a Review’, unpublished paper, 2017.

[20] C. F. Leroy, ‘Second International Geodetic Symposium on Satellite Doppler Positioning’, *Bull. Géod.*, vol. 53, no. 2, pp. 185–190, Jun. 1979.

[21] T. J. Ford and J. Hamilton, ‘A New Positioning Filter: Phase Smoothing in the Position Domain’, *Navigation*, vol. 50, no. 2, pp. 65–78, 2003.

[22] K. Krasuski and D. Wierzbicki, ‘Monitoring Aircraft Position Using EGNOS Data for the SBAS APV Approach to the Landing Procedure’, *Sensors*, vol. 20, p. 1945, Mar. 2020.

[23] F. Lecomte, ‘The erroneous GPS signal’. [Online]. Available: https://www.reflexions.uliege.be/cms/c_358355/en/the-erroneous-gps-signal?part=2. [Accessed: 10-Apr-2021]

[24] I. Webster, ‘A regional model for the prediction of ionospheric delay for single frequency users of the Global Positioning System’, Apr. 1993.

[25] G. S. Kumar, G. S. B. Rao, and M. N. V. S. S. Kumar, ‘GPS Signal Short-Term Propagation Characteristics Modeling in Urban Areas for Precise Navigation Applications’, *Positioning*, vol. 4, no. 2, pp. 192–199, May 2013.

[26] R. Santerre, A. Geiger, and S. Banville, ‘Geometry of GPS dilution of precision: revisited’, *GPS Solut.*, vol. 21, no. 4, pp. 1747–1763, Oct. 2017.

[27] Maurizio Scaramuzza, ‘Presentation Satellite Constellations, unpublished’, Zurich, ZHAW SoE, 2021.

[28] International Civil Aviation Organization (ICAO), ‘Guide for Ground Based Augmentation System Implementation’, p. 31, Mar. 2013.

[29] International Civil Aviation Organization (ICAO), *Aeronautical Telecommunication Annex 10*. 2018.

[30] F. Corraro, U. Ciniglio, P. Canzolino, L. Garbarino, S. Gaglione, and V. Nastro, ‘An EGNOS Based Navigation System for Highly Reliable Aircraft Automatic Landing’, 2009.

[31] R. Sabatini, T. Moore, and S. Ramasamy, ‘Global Navigation Satellite Systems Performance Analysis and Augmentation Strategies in Aviation’, *Prog. Aerosp. Sci.*, vol. 95, Nov. 2017.

[32] SKYbrary, ‘Ground Based Augmentation System (GBAS) - SKYbrary Aviation Safety’, 08-Feb-2021. [Online]. Available: https://www.skybrary.aero/index.php/Ground_Based_Augmentation_System_(GBAS). [Accessed: 20-Feb-2021]

[33] T. Yoshihara, S. Saito, A. Kezuka, K. Hoshinoo, S. Fukushima, and S. Saitoh, ‘Development of a Ground Subsystem Prototype for Ground-Based Augmentation System (GBAS) Approach Service Type D (GAST-D) and the Evaluation of Its Performance in a Low Magnetic Latitude Region’, in *Air Traffic Management and Systems III*, Singapore, 2019, pp. 138–151.

[34] GMV, ‘GBAS Fundamentals - Navipedia’, 2011. [Online]. Available: https://gssc.esa.int/navipedia/index.php/GBAS_Fundamentals. [Accessed: 28-Feb-2021]

[35] A. El-Rabbany, *Introduction to GPS: The Global Positioning System*. Artech House, 2002.

[36] GMV, ‘SBAS Fundamentals - Navipedia’, 2011. [Online]. Available: https://gssc.esa.int/navipedia/index.php/SBAS_Fundamentals. [Accessed: 23-Feb-2021]

[37] P. J. G. Teunissen and O. Montenbruck, Eds., *Springer Handbook of Global Navigation Satellite Systems*. Springer International Publishing, 2017 [Online]. Available: https://www.springer.com/gp/book/9783030731724. [Accessed: 06-Mar-2021]

[38] H. Yoon, H. Seok, C. Lim, and B. Park, ‘An Online SBAS Service to Improve Drone Navigation Performance in High-Elevation Masked Areas’, *Sensors*, vol. 20, no. 11, May 2020 [Online]. Available: https://www.ncbi.nlm.nih.gov/pmc/articles/PMC7309144/. [Accessed: 07-Jun-2021]

[39] N. Jakowski *et al.*, ‘Behaviour of large scale structures of the electron content as a key parameterfor range errors in GNSS applications’, Jan. 2009.

[40] Wikipedia, ‘Datei:EGNOS map.svg’, Picture. [Online]. Available: https://commons.wikimedia.org/wiki/File:EGNOS_map.svg. [Accessed: 29-Apr-2021]

[41] Z. Nie, P. Zhou, F. Liu, Z. Wang, and Y. Gao, ‘Evaluation of Orbit, Clock and Ionospheric Corrections from Five Currently Available SBAS L1 Services: Methodology and Analysis’, *Remote Sens.*, vol. 11, no. 4, p. 411, Jan. 2019.

[42] RTCA, *Minimum Operational Performance Standards For Global Positioning System/Wide Area Augmentation System Airborne Equipment, DO-229D*. 2006.

[43] DLR, ‘ATRA Neue Dimensionen in der Luftfahrtforschung’. [Online]. Available: https://www.dlr.de/content/de/downloads/publikationen/broschueren/2016/atra-neue-dimensionen-luftfahrtforschung.pdf?__blob=publicationFile&v=12. [Accessed: 06-Jun-2021]

[44] EUROCONTROL, ‘PEGASUS Interface Control Document’. Navigation Domain GNSS Activity, 27-Nov-2018.

[45] GMV, ‘Integrity - Navipedia’, 2011. [Online]. Available: https://gssc.esa.int/navipedia/index.php/Integrity. [Accessed: 06-May-2021]

[46] H.-P. Sanz, M, J. J.M, T. A, and D. I, ‘The Stanford – ESA Integrity Diagram: Focusing on SBAS Integrity - Navipedia’, 2006. [Online]. Available: https://gssc.esa.int/navipedia/index.php/The_Stanford_%E2%80%93_ESA_Integrity_Diagram:_Focusing_on_SBAS_Integrity. [Accessed: 06-Jun-2021]

[47] GMV, ‘EGNOS Future and Evolutions - Navipedia’, 2011. [Online]. Available: https://gssc.esa.int/navipedia/index.php/EGNOS_Future_and_Evolutions. [Accessed: 06-Jun-2021]

[48] EUSPA, ‘Project launched to determine benefits of EGNOS V3 high accuracy service | European GNSS Service Centre’. [Online]. Available: https://www.gsc-europa.eu/news/project-launched-to-determine-benefits-of-egnos-v3-high-accuracy-service. [Accessed: 06-Jun-2021]

Appendix

The Appendix consists of a short Manual on how to use the PEGASUS program.

Converter

Important: verify that “GPS week roll-over” is well set for the time-period of your observations (week numbers crossing the value 1023).

Standalone GNSS

- Input File

→ xx.yyo (xx = flight, yy = Date, e.g. F0595.19o) and the associated ephemeris file xx.yyN (should have the same prefix e.g. F0595.19N)

- Data Properties

→ Receiver: RINEX Format or automatic

→ Correction mode: SBAS Mode 0

After that you get the following files:

*Range file ‘*_cnv.rng’ file which can be further processed (Pegasus GNSS Solution) to get the position solution.*

GBAS

1) PacketDecoder: The starting point is a CAP file, which must first be entered into the PacketDecoder and the following steps must be done:

- Get into the "dist" directory
- copy the CAP file you want to decode inside this directory
- Edit the "run.bat" file
- Replace the filename "example.cap" by the name of your CAP file
- Start the run.bat program

After that you will get the following files:

- *One file called ‘*.vdb.out’: It contains GBAS messages*
- *Several files called ‘*.rsmu.out’: They contain the observations data*

2) Pegasus Converter (VDB file)

- Input File

→ ‘*.vdb.out’ from the PacketDecoder

- Data Properties

→ Receiver: GBAS VDB

→ Correction mode: GBAS ignores slot delay (for VDB receiver without PPS sync)

After that you get the following files:

- *Message types* ‘*.gmt’ *which can then be applied to the observations to get the GBAS corrected position solution.*

3) Pegasus Converter (rsmu files) This step is only needed if the antenna position solution is needed.

- Input File

→ ‘*.rsmu.out’ from the PacketDecoder

- Data Properties

→ Receiver: CMA-4048

→ Correction mode: GBAS ignore slot delay (for VDB receiver without PPS sync)

After that you get the following files:

*Range file ‘*_cnv.rng’ which can be further processed (Pegasus GNSS Solution) to get for example the position solution of the rsmu Antenna.*

SBAS

The files ‘xx.yyB’, ‘xx,yyn’ and ‘xx,yyo’ (xx = flight, yy = date) must be in the same folder and have the same prefix. e.g. F0595.19B, F0595.19n and F0595.19o.

After that one of the files can be read into the Pegasus Converter (it does not matter which one).
- Data Properties
→ Receiver: RINEX Format
→ Correction mode: SBAS Mode 0
After that you get the following files:
*Range file '*_cnv.rng' which can be further processed (Pegasus GNSS Solution) and the SBAS message files '*.smt' which can be applied to the '*_cnv.rng' file to get the SBAS corrected position solution.*

GNSS Solution

Verify that for the differential corrections (GBAS and SBAS) the time of the message files corresponds to the DOY (Day Of Year) of the time period of your observations. (Everything that is not mentioned can remain in the default settings)

Standalone Position Solution

- Input File
→ '*_cnv.rng'
- General Options
→ GPS
- Advanced…
→ Set the Smoothing constant on 100 seconds
→ Max Divergence Repetition 3 samples
→ Set the Max Data Gap on 0.01 seconds
→ Min. Elevation 5 deg

GBAS Position Solution

Check that both ranging measurements '*_cnv.rng' and messages files '*vdb.gxx' in output of Convertor have the same file prefix.
- Input File
→ '*_cnv.rng'
- General Options
→ GBAS
→ select the box "External Messages" and choose the messages files '*.gmt'
- Advanced…
→ Set the Smoothing constant on 100 seconds
→ Set the Max Data Gap on 100 seconds (GBAS has a bigger data gap and if it is too small the corrections will not be applied)
→ Min. Elevation 5 deg

SBAS Position Solution

If you are working with EDAS EGNOS messages, check that both ranging measurements '*_cnv.rng' and messages files '*.sxx' in output of Convertor have the same file prefix.
- Input File
→ '*_cnv.rng' file
- General Options
→ SBAS
→ Choose a GEO, verify that the GEO you choose was operational during the time period of your observations https://egnos-user-support.essp-sas.eu/new_egnos_ops/
→ select the box "External Messages" and choose the messages files '*.smt'
- Advanced…
→ In the column SV Selection, all boxes can remain active.
→ Set the Smoothing constant on 100 seconds
→ Set the Max Data Gap on 100 seconds (SBAS has a bigger data gap if it is too small the corrections will not be applied)
→ Min. Elevation 5 deg
→ Nonstandard SBAS options: choose the box "ignore almanac" if you don't have almanac files.